Impacts of Nucleating Aerosol on Florida Storms. Part I: Mesoscale Simulations

SUSAN C. VAN DEN HEEVER, GUSTAVO G. CARRIÓ, WILLIAM R. COTTON, PAUL. J. DEMOTT, AND ANTHONY J. PRENNI

Colorado State University, Fort Collins, Colorado

(Manuscript received 8 September 2004, in final form 1 November 2005)

ABSTRACT

Toward the end of the Cirrus Regional Study of Tropical Anvils and Cirrus Layer–Florida Area Cirrus Experiment (CRYSTAL–FACE) field campaign held during July 2002, high concentrations of Saharan dust, which can serve as cloud condensation nuclei (CCN), giant CCN (GCCN), and ice-forming nuclei (IFN) were observed over the peninsula of Florida. To investigate the impacts of enhanced aerosol concentrations on the characteristics of convective storms and their subsequent anvil development, sensitivity tests are conducted using the Regional Atmospheric Modeling System (RAMS) model, in which the initialization profiles of CCN, GCCN, and IFN concentrations are varied. These variations are found to have significant effects on the storm dynamics and microphysical processes, as well as on the surface precipitation. Updrafts are consistently stronger as the aerosol concentrations are increased. The anvils cover a smaller area but are better organized and have larger condensate mixing ratio maxima in the cases with greater aerosol concentrations. Cloud water mass tends to increase with increasing aerosol concentrations, with enhanced GCCN concentrations having the most significant influence. Increasing either the GCCN or IFN concentrations produces the most rainfall at the surface whereas enhanced CCN concentrations reduce surface rainfall. Higher IFN concentrations produce ice at warmer temperatures and deeper anvils, but simultaneously increasing the concentrations of CCN and GCCN leads to more supercooled liquid water available for freezing and greater ice mixing ratios. Graupel mixing ratios decrease and hail mixing ratios increase with increasing aerosol concentrations. Higher concentrations of GCCN and IFN result in greater accumulated surface precipitation initially. By the end of the simulation period, however, the accumulated precipitation is the greatest for the case in which the aerosol concentrations are lowest. Such changes in the dynamical and microphysical characteristics of convective storms as a result of the variations in aerosol concentrations have potential climate consequences, both through cloud radiative effects and the hydrological cycle. The impacts of varying CCN, GCCN, and IFN concentrations on the anvils will be discussed more fully in Part II.

1. Introduction

Hydrometeor formation and precipitation processes within clouds depend strongly on the presence of aerosols, in particular, CCN, GCCN, and IFN. However, aerosols, whether natural or anthropogenic, affect the climate both directly through the absorption and scattering of solar radiation and indirectly by modifying cloud properties that are associated with cloud radiative feedback effects. The indirect effect of aerosols on climate is still not well understood in spite of numerous modeling and observational studies. This may be attributed to the sheer number and scale of the dynamical, microphysical and chemical processes involved, as well as to the difficulty in obtaining in situ measurements that demonstrate this effect conclusively.

The indirect aerosol effect is generally attributed to Twomey (1977), although differences between the droplet concentrations and size distributions of continental and maritime clouds had already been observed about 20 years earlier (Squires 1956, 1958). Twomey (1977) and Twomey et al. (1984) suggested that under conditions of equivalent liquid water content (LWC), increasing the concentrations of atmospheric aerosol results in greater concentrations of CCN, higher cloud droplet concentrations, smaller droplet sizes, increases in cloud optical depth and albedo, and hence more reflective clouds. This Twomey effect may be similar in magnitude but opposite in sign to the greenhouse ef-

Corresponding author address: Susan C. van den Heever, Dept. of Atmospheric Science, Colorado State University, Fort Collins, CO 80523-1371.
E-mail: sue@atmos.colostate.edu

fect. Albrecht (1989) proposed that precipitation is suppressed when the number of CCN are increased, and that this results in more reflective clouds as the cloud droplets are smaller and the liquid water path (LWP) greater. Kaufman and Nakajima (1993) found that the ingestion of smoke into clouds over Brazil leads to smaller cloud droplets and optically thicker clouds. Work by Jiang et al. (2002), however, showed that the entrainment of pollution into stratocumulus clouds may under certain conditions reduce the LWP as a consequence of modulations in drizzle rates, thereby decreasing the cloud reflectivity.

Precipitation production may also be significantly affected by the ingestion of aerosols such as urban and industrial pollution, as well as smoke from forest fires and other burning vegetation. Greater concentrations of CCN result in the production of many more small cloud droplets, narrower cloud droplet spectra, and reduced collision efficiencies, all of which act to inhibit precipitation processes, and may even completely shut off precipitation at times (Kaufman and Nakajima 1993; Borys et al. 1998; Rosenfeld and Lensky 1998; Rosenfeld 1999, 2000; Andreae et al. 2004). It has also been suggested, based on statistical analyses, that air pollution may enhance precipitation in near-coastal Atlantic Ocean areas (Cerveny and Balling 1998).

The effects of GCCN on cloud characteristics and precipitation processes have received relatively little attention compared with CCN. Unlike CCN, GCCN appear to enhance precipitation (Hobbs et al. 1970; Eagan et al. 1974; Dettwiller and Changnon 1976; Hindman et al. 1977a,b; Braham et al. 1981; Mather 1991) through the broadening of the cloud droplet spectrum, which enhances the efficiency of collision and coalescence processes. Feingold et al. (1999) found evidence that the presence of GCCN can change a nonprecipitating stratocumulus cloud into a precipitating cloud, and that the relative impact of the GCCN on the formation of drizzle increases with increasing CCN concentrations. They also found that the presence of GCCN significantly moderates the CCN effects on cloud optical properties. Laird et al. (2000) demonstrated that the efficiency of the initial development of precipitation in small Florida cumuli was enhanced by the presence of ultragiant nuclei, which can immediately act as embryos for raindrop growth after entering cloud base. Over cities, the aerosols that may serve as GCCN are often removed from pollution emissions by filtering.

Dust is transported from major desert regions all around the globe, thereby influencing the aerosol composition and concentrations in locations far removed from their source (Prospero 1996, 1999). Asian dust regularly affects Hawaii and the western United States (Perry et al. 1999; Sassen 2002), and Perry et al. (1997) found that dust plumes from North Africa affected the eastern United States on average of 3 times per year during the summer months from 1992 to 1995, with each event lasting about 10 days. Large quantities of dust from North Africa are also carried into Florida every summer, with daily concentrations ranging from 10 to 100 $\mu g\ m^{-3}$ (Prospero 1999). Prospero (1999) found from 23 yr of data taken in Miami, Florida, that dust events over Florida typically last several days or longer, with maximum concentrations occurring in July, and relatively high concentrations also occurring in June and August.

Dust can directly affect weather and climate by absorbing and scattering solar and infrared radiation (Quijano et al. 2000). This can enhance the trade wind inversion and generate a dry well-mixed layer that can extend to nearly 500 mb (Prospero and Carlson 1972). Recently Dunion and Velden (2004) provided convincing evidence that Saharan dust can have a substantial impact on Atlantic hurricane activity. Dust can also serve as CCN, GCCN, and IFN, and as such can have conflicting consequences on cloud radiative properties and rainfall. Rosenfeld et al. (2001), for example, present evidence that dust suppresses rainfall by virtue of serving as CCN and producing numerous small droplets. On the other hand, Levin et al. (1996) show through modeling studies that dust can become coated with sulfates and thereby act not only as CCN, but GCCN as well. They suggest that the increased concentrations of GCCN will enhance precipitation. This is supported by the satellite observations of Rosenfeld et al. (2002) that show clouds in polluted air are nonprecipitating over land but rapidly transform into precipitating clouds once the air mass advects over the sea and sea salt particles (GCCN) become entrained into the clouds. The results of a recent study by Mahowald and Kiehl (2003), in which large-scale, long-term satellite datasets and surface dust observations were compared, suggest that precipitation is suppressed in thin low-altitude clouds, but enhanced in high-altitude clouds over the west coast of North Africa and the adjacent Atlantic Ocean.

It has been known for some time from laboratory studies that dust can serve as efficient IFN (Schaefer 1949, 1954; Isono et al. 1959; Roberts and Hallett 1968; Zuberi et al. 2002; Hung et al. 2003). IFN measurements by Gagin (1965) and Levi and Rosenfeld (1996) show further that desert dust is an effective IFN. Rosenfeld and Nirel (1996) suggest that desert dust serving as GCCN and IFN can enhance precipitation and thereby influence the interpretation of the effectiveness of cloud seeding experiments.

More recently, during the Cirrus Regional Study of Tropical Anvils and Cirrus Layers–Florida Area Cirrus Experiment (CRYSTAL–FACE) field program conducted by the National Aeronautics and Space Administration (NASA; Jensen et al. 2004) over the Florida Peninsula, Sassen et al. (2003) showed using aircraft and lidar data that a mildly supercooled altocumulus cloud over southern Florida was glaciated in the presence of Saharan dust, which formed effective IFN. During the same field program DeMott et al. (2003) found extremely high concentrations of IFN (in excess of 1 cm^{-3} for particles less than 1 μm in size) within dust layers over Florida, confirming the efficiency of dust aerosols in the nucleation of ice. It is clear that dust can substantially alter the microstructure of clouds in a variety of ways.

The goal of the CRYSTAL–FACE program was to investigate the formation and characteristics of subtropical thunderstorms and their associated cirrus clouds, and the effects that these systems have on the troposphere and lower stratosphere. During the field phase of this program, held over the Florida Peninsula during July 2002, high aerosol concentrations were observed on 28 and 29 July. These appear to be associated, certainly in part, with the penetration of Saharan dust over the peninsula during this time (DeMott et al. 2003; Sassen et al. 2003). The CRYSTAL–FACE field program thus provided an ideal opportunity to examine the impacts of dust on the convective and anvil stages of convection over Florida, as measurements were taken on days on which there was relatively little dust, and on days during which the dust concentrations were high, thus providing a basis for comparison. The goal of the research presented here is thus to investigate the impacts that variations in the concentrations of CCN, GCCN, and IFN may have on the characteristics of the convective and anvil stages of Florida convection. This goal is to be achieved using the observations made during the CRYSTAL–FACE field campaign and a cloud-resolving numerical model.

The setup of the mesoscale numerical model used to conduct the simulations, the initialization procedures of the model and the experiment design are discussed in section 2 of this paper. Results of the modeling sensitivity tests are presented in section 3, and a summary of our findings and the conclusions drawn are included in section 4. This paper is the first in a two-part series, the focus of which is on the bulk microphysical and dynamical characteristics associated with convection on the cloud scale. In the second part (Carrió et al. 2006, hereafter Part II), a large-eddy simulation (LES) model, initialized with the cloud-resolving output discussed in this paper, is used to investigate the microphysical characteristics and radiative processes of the anvils in more detail.

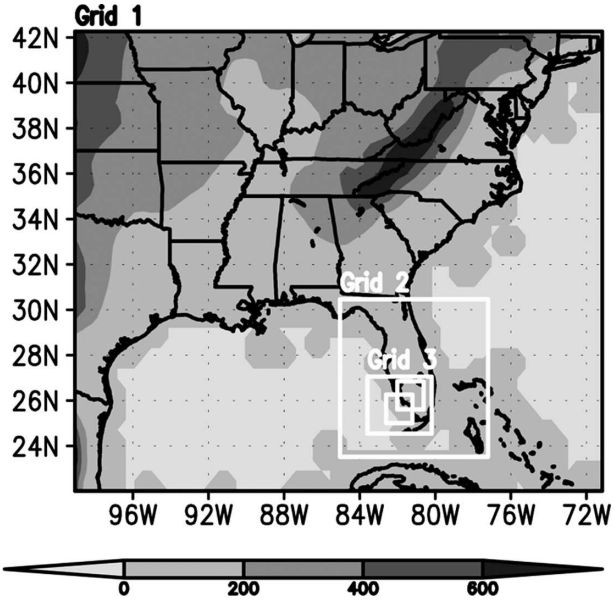

FIG. 1. The locations of grids 1 through 4. Both locations of grid 4 are indicated.

2. Model and experiment setup

a. Model configuration

The Regional Atmospheric Modeling System (RAMS; Pielke et al. 1992; Cotton et al. 2003) developed at Colorado State University (RAMS@CSU) was used in this study. Four two-way interactive nested model grids with horizontal grid spacings of 50, 10, 2, and 0.5 km were employed (Fig. 1). The size of the fourth grid was limited because of computer memory constraints and had to be moved to ensure that the convective cores being simulated remained within this grid. Both locations of grid 4 are shown in Fig. 1. Thirty-six vertical levels with variable grid spacing were used, and the model top extended to approximately 20 km above ground level (AGL). The long time step was 60 s.

The basic radiative condition (Klemp and Wilhelmson 1978) was applied to the normal velocity components at the lateral boundaries of grid 1. RAMS was heterogeneously initialized with 40-km Eta data from 28 July 2002. These data were also used as time-dependent fields to which the lateral boundary regions of grid 1 are nudged during integration. The surface processes were parameterized using the Land Ecosystem–Atmosphere Feedback 2 (LEAF-2; Walko et al. 2000). A 40-class vegetation dataset from the United States Geological Survey (USGS) with a spatial resolution of 100 m over Florida was incorporated into this

TABLE 1. RAMS model configuration and options.

Model aspect	Setting
• Grid	• Arakawa C grid (Mesinger and Arakawa 1976) • Four grids • Horizontal grid: Grid 1: $\Delta x = \Delta y = 50$ km 60×50 points Grid 2: $\Delta x = \Delta y = 10$ km 82×82 points Grid 3: $\Delta x = \Delta y = 2$ km 177×147 points Grid 4: $\Delta x = \Delta y = 0.5$ km 290×290 points • Vertical grid: Δz variable 36 vertical levels • Model top: ~20 km • Seven levels below 1 km AGL
• Initialization	• 40 km Eta data • Aerosol profiles obtained from CRYSTAL–FACE field campaign
• Time step	• 60 s
• Simulation duration	• 12 h
• Microphysics scheme	• Two-moment bulk microphysics (Meyers et al. 1997) • Water species: vapor, cloud water, rain, pristine ice, snow, aggregates, graupel, and hail all activated
• Convective initiation	• Kuo (Kuo 1974; Molinari 1985) cumulus parameterization scheme on grids 1 and 2; explicit convection on grids 3 and 4
• Boundary conditions	• Radiative lateral boundary (Klemp and Wilhelmson 1978)
• Turbulence scheme	• Mellor and Yamada (1974) level 2.5 scheme on grids 1–3; Smagorinsky (1963) deformation-K closure scheme with stability modifications by Lilly (1962) and Hill (1974) on grid 4
• Radiation scheme	• Harrington (1997)
• Surface scheme	• LEAF-2 (Walko et al. 2000)

scheme, the details of which are described by Marshall et al. (2004). Standing water was allowed on the appropriate vegetation categories (Kushlan 1990), which is important for the Everglade regions of Florida. Radiation was parameterized using Harrington's (1997) scheme.

Convection was explicitly resolved on grids 3 and 4, but was parameterized on grids 1 and 2 using a modified Kuo cumulus parameterization scheme (Kuo 1974; Molinari 1985). The mixing ratios and number concentrations of the various hydrometeors were predicted through the use of a two-moment bulk microphysical scheme (Meyers et al. 1997), and all the available water species were activated (pristine ice, snow, aggregates, graupel, hail, cloud water and rain). In the new two-moment scheme the cloud droplet spectrum is decomposed into two modes, one called c1, which is for droplets 1 to 40 μm in diameter, and the second called c2, which is for droplets 40 to 80 μm in diameter. Collection is simulated using stochastic collection equation solutions, facilitated by lookup tables, rather than by continuous accretion approximations. The philosophy of bin representation of collection is extended to calculations of drop sedimentation. Explicit activation of CCN, GCCN, and IFN are simulated based on Saleeby and Cotton (2004). The aerosol species within the model are initialized horizontally homogeneously with vertical profiles of CCN, GCCN, and IFN concentrations, the details of which are covered in the next section. The concentrations of these aerosol species are prognosed in RAMS. The model configuration used for the simulations presented here is summarized in Table 1.

b. Experiment design

On 28 July 2002, a high dust day during the CRYSTAL–FACE field campaign, an easterly wave penetrated over the southern Florida Peninsula, transporting Saharan desert dust to this region. Storms initially developed to the south and southwest of Lake Okeechobee, enhanced by the presence of the easterly wave (Fig. 2). These storms continued to strengthen, accompanied by the development of new convection, and progressed in a westward to southwestward direction, reaching the coastal regions of Everglade City and Fort Meyers between 2100 and 2200 UTC. Convection started to weaken after ~2200 UTC, leaving the remnant anvils extending over the oceans for several more hours.

To simulate the impacts of varying aerosol concentrations on the convective development and resultant anvils, idealized vertical profiles of the aerosol concentrations were established based on measurements made

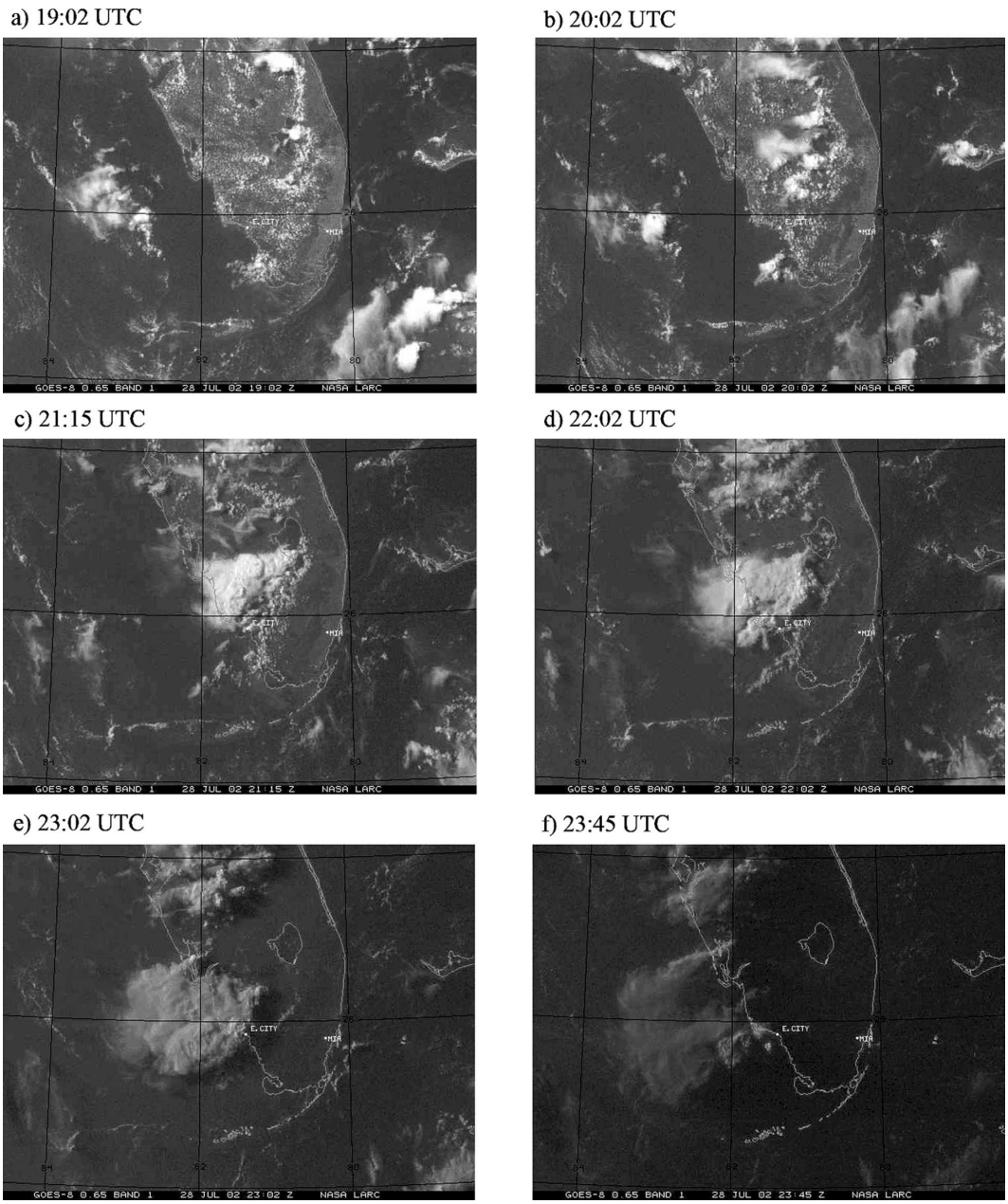

FIG. 2. Visible satellite imagery of the storm development over the Florida Peninsula at approximately hourly intervals on 28 Jul 2002 (figures used with the permission of L. Nguyen, NASA Langley Research Center).

on relatively clean and dusty days during the field campaign. For the clean or control case, measurements from 18 July were used for IFN, while a selection of days for which strong dust influences were not present based on Sassen et al. (2003) provided a composite of clean vertical profiles for other aerosols. Data from 28 July were used for the dusty case. CLN and OBS will be used throughout this paper to designate these cases, respectively.

The IFN measurements were obtained from the continuous flow diffusion chamber (CFDC) on board the Citation aircraft, the design and characteristics of which have been described by Rogers et al. (2001). The measurements used, collected during clear-air sampling, were taken at approximately −37°C and ~86% (123%) relative humidity with respect to water (ice) within the dust layer on 28 July, while those on 18 July were made at approximately −24°C and 134% relative humidity with respect to ice (DeMott et al. 2003). Two factors support a relatively constant IFN concentration initial-

ization profile versus altitude in the CLN case. First, the maximum IFN concentrations at constant processing conditions that are shown by DeMott et al. (2003) for 18 July did not vary greatly with altitude to 8 km, and additional data collected in clear air at 10 km on this day support that this result was also valid to higher altitudes. Second, vertical profiles of integrated aerosol concentrations at sizes above 0.1 μm (obtained using the cloud aerosol spectrometer described below), the size regime from which IFN predominantly derive (Chen et al. 1998), indicated on average for clean days, nearly constant concentrations between 4 and 12 km. The upper regions of the idealized vertical IFN profiles were therefore kept constant with height up to the tropopause, above which they were systematically decreased. The CLN and OBS vertical IFN profiles used to initialize the model are shown in Fig. 3c. The vertical profiles are multiplied by a function of the base state density during the model initialization process and thus will moderately decrease with height in the middle and upper levels.

In RAMS the number of pristine ice crystals formed by deposition–condensation freezing on IFN is given by

$$N_{\text{pris}} = N_{\text{IFN}} F_M, \tag{1}$$

where F_M is a function of the Meyers et al. (1992) formula that represents the fraction of available IFN that are activated as a function of ice supersaturation, and N_{IFN} is the maximum concentration of IFN available for activation. Here, F_M is maximized (equal to 1) for these simulations at an ice supersaturation of 40%. The variable N_{IFN} is a forecast variable that is initialized using the idealized profiles just presented. Then N_{IFN} is advected and diffused and has sinks due to ice activation. We note that the CLN N_{IFN} profile is nearly equivalent to assuming the standard Meyers et al. (1992) IFN concentration dependence on supersaturation. The OBS profile is a more conservative estimate of dust impacts on IFN concentration because the measurements on this day were made at ice supersaturations of 23%. However, the use of greater IFN concentrations would simply have served to enhance the responses presented below.

CCN measurements up to ~3.5 km AGL were made using a continuous flow CCN instrument on board the Twin Otter aircraft (VanReken et al. 2003) at supersaturations of 0.3% and 0.7%, the latter of which was used for our purposes. VanReken et al. validated that an assumption of single composition aerosols was generally valid for relating CCN supersaturation to aerosol size during CRYSTAL–FACE. We therefore applied this assumption at higher altitudes where smaller size

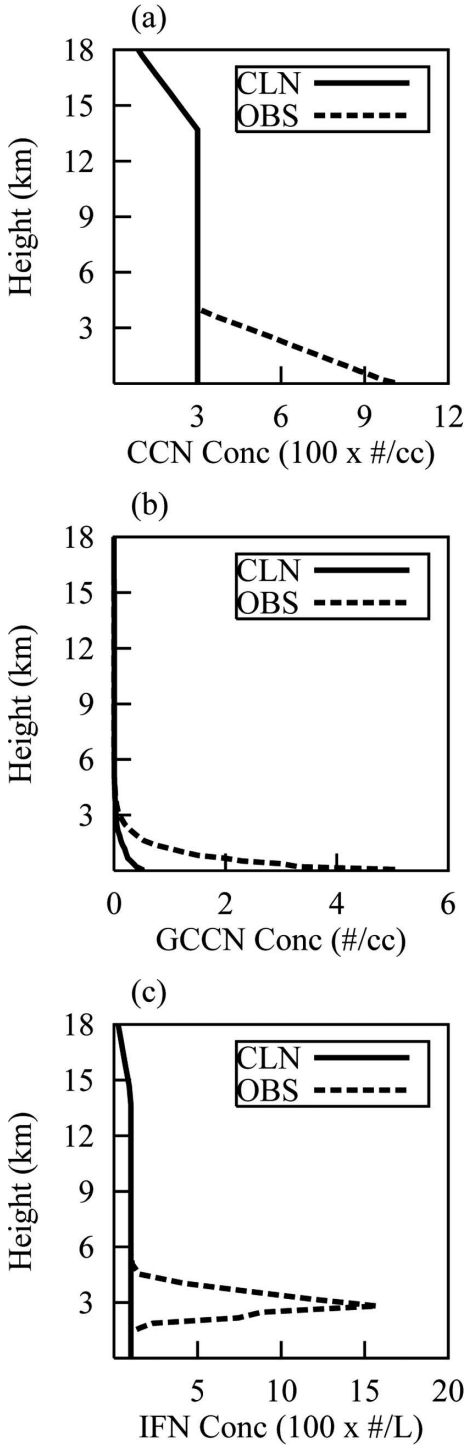

FIG. 3. Idealized vertical (a) CCN, (b) GCCN, and (c) IFN profiles used to initialize the model.

(<100 nm) aerosol data were available from the University of Denver Nucleation-Mode Aerosol Sizing Spectrometer (N-MASS) (Lee et al. 2004) on board the WB-57 aircraft. CCN concentrations in the mid- to up-

per levels were thereby estimated from the aerosol data to compose the vertical profile shown in Fig. 3a. It should be noted that the measured CCN concentrations in the lower levels varied significantly in time and space throughout the field project. However, consistently higher CCN concentrations in the lower levels were a particular feature of high dust days, while only an irregular feature of the cleaner days. Idealized vertical profiles with high and low CCN concentrations in the lower levels were therefore used for the dusty and clean days, respectively (Fig. 3a).

In RAMS the concentration of CCN nucleated to become cloud droplets is obtained from a lookup table as a function of CCN concentration, vertical velocity, and temperature (Saleeby and Cotton 2004). The lookup table is generated previously (offline) from detailed parcel-bin model calculations. Essentially, the number of droplets nucleated per unit volume follows the equation

$$N_{c1} = N_{CCN} S_w^b, \tag{2}$$

where N_{CCN} is the concentration of CCN, N_{c1} represents the concentration of cloud droplets activated in the first cloud droplet mode (droplets with diameters less than 40 μm), S_w is water supersaturation, and b is an empirically determined parameter. The model forecast variable N_{CCN} can be advected and diffused. It also has sinks due to nucleation to form cloud droplets and sources as cloud droplets are evaporated.

The instrument used to determine the GCCN was the Droplet Measurement Technologies' (DMT; http://www.dropletmeasurement.com) cloud aerosol spectrometer (CAS) on board the WB-57 aircraft, which is capable of measuring sizes from 0.3 to 50 μm (Baumgardner et al. 2001). The sampling efficiency for particles above 3 μm is determined by sample volume, which is $\sim$25 cm^3 s^{-1}, so the uncertainty is quite large for measuring numbers as low as 10^{-4} cm^{-3}. Ascent and descent profiles were used to determine the idealized GCCN vertical profile, with any aerosol particle falling into the size range of 1 to 50 μm being assumed to be wettable and activated as cloud2 mode droplets whenever the cloud is supersaturated with respect to water. The nucleation is based on

$$N_{c2} = N_{GCCN}; \quad S_w > 0.0, \tag{3}$$

where N_{c2} represents the concentration of cloud droplets in the second cloud droplet mode (diameters between 40 and 80 μm), and N_{GCCN} is the concentration of GCCN. Here, N_{GCCN} is also a forecast variable in RAMS and is advected and diffused by the model. Its major sink is activation of cloud droplets N_{c2} into the cloud2 mode. The idealized vertical GCCN profiles used to initialize the model for the CLN and OBS cases are shown in Fig. 3b.

TABLE 2. Aerosol initialization profiles for the sensitivity tests described in the text.

Experiment	Name	IFN	CCN	GCCN
Exp1	CLN	Clean	Clean	Clean
Exp2	GCCN	Clean	Clean	Observed
Exp3	CCN	Clean	Observed	Clean
Exp4	IFN	Observed	Clean	Clean
Exp5	C + G	Clean	Observed	Observed
Exp6	I + G	Observed	Clean	Observed
Exp7	I + C	Observed	Observed	Clean
Exp8	OBS	Observed	Observed	Observed

Numerous sensitivity tests were conducted using RAMS in order to investigate the response of the convection and subsequent anvil development to varying aerosol concentrations, as well as to provide boundary conditions for the LES model. The sensitivity tests used for the LES model are described in detail in Part II and will not be covered here. For the storm-scale sensitivity tests presented here, all of the model simulations were run for 12 h from 1200 to 0000 UTC (0800 to 2000 LT) on 28 July 2002, having all been initialized with synoptic data from 28 July 2002. The simulations were run with three grids from 1200 to 1800 UTC, after which the fourth grid was added.

Eight sensitivity tests were performed in which various combinations of the CLN and OBS initialization profiles of the three aerosol species were used. The sensitivity tests were identical in all other respects. In the control experiment (CLN), the clean profiles for all three aerosol species were utilized, while the OBS profiles for all three aerosol species were used for the OBS experiment. The combinations of the profiles used to initialize the model in the six other sensitivity tests are shown in Table 2. In investigating the influences of aerosol variations on the convective storm characteristics, the approach used here is one of a cloud-ensemble or LES-type philosophy, in that the focus is not on trying to replicate any single convective storm or cell, but rather on the ensemble characteristics of the clouds and storms.

Finally, a factor separation analysis was performed using all eight sensitivity tests (Stein and Alpert 1993). The formulation of each factor is shown in Table 3. This type of analysis is useful in that it gives the contribution made by each aerosol species individually, as well as the contributions made by the interactions between the species to a field of interest. The results of the sensitivity tests and the factor analysis will now be presented.

TABLE 3. The components of the factor separation analysis described in the text.

Factor	Name	Description	Calculation
f_0	OBS	Part of the predicted field independent of the factors (clean air profiles)	f_0 = exp1
f_1	IFN	Part of the predicted field when only factor number 1 (IFN) is fully switched on	f_1 = exp4 − exp1
f_2	CCN	Part of the predicted field when only factor number 2 (CCN) is fully switched on	f_2 = exp3 − exp1
f_3	GCCN	Part of the predicted field when only factor number 3 (GCCN) is fully switched on	f_3 = exp2 − exp1
f_{12}	I + C	Part of the predicted field dependent solely on the combination of factors 1 and 2 (IFN and CCN)	f_{12} = exp7 − (exp4 + exp3) + exp1
f_{13}	I + G	Part of the predicted field dependent solely on the combination of factors 1 and 3 (IFN and GCCN)	f_{13} = exp6 − (exp4 + exp2) + exp1
f_{23}	C + G	Part of the predicted field dependent solely on the combination of factors 2 and 3 (CCN and GCCN)	f_{23} = exp5 − (exp3 + exp2) + exp1
f_{123}	I + C + G	Part of the predicted field dependent solely on the combination of factors 1, 2, and 3 (IFN, CCN, and GCCN)	f_{123} = exp8 − (exp7 + exp6 + exp5) + (exp4 + exp3 + exp2) − exp1

3. Aerosol sensitivity tests

a. Storm system development

Vertically integrated condensate for the CLN and OBS cases are shown in Figs. 4 and 5, respectively. In both cases convection (associated with regions of greater vertically integrated condensate) develops to the southwest of Lake Okeechobee and tracks toward the west and southwest, as is evident in the satellite imagery (Fig. 2). Extensive anvil cirrus clouds develop in both simulations. Comparing the CLN and OBS simulations it is apparent that the anvil in the OBS case covers a smaller area but achieves greater maximum condensate amounts and is better organized than in the CLN case. The OBS is also a better representation of the actual observations. Increasing the aerosol concen-

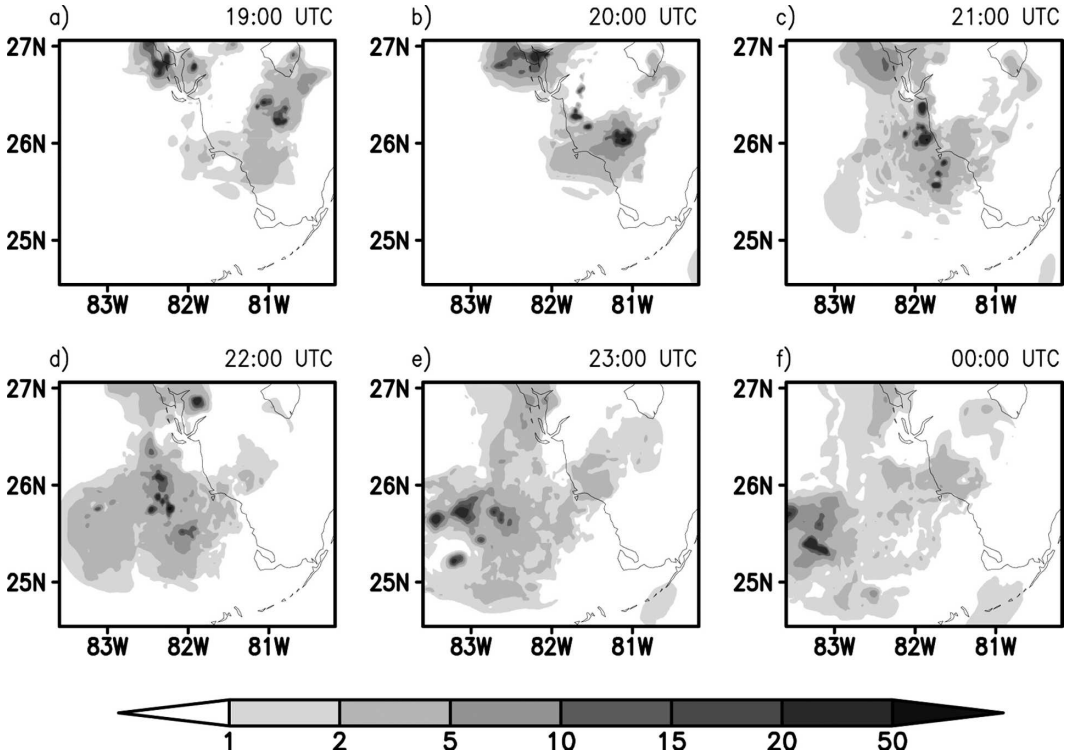

FIG. 4. Vertically integrated condensate (mm) at hourly intervals for the CLN experiment.

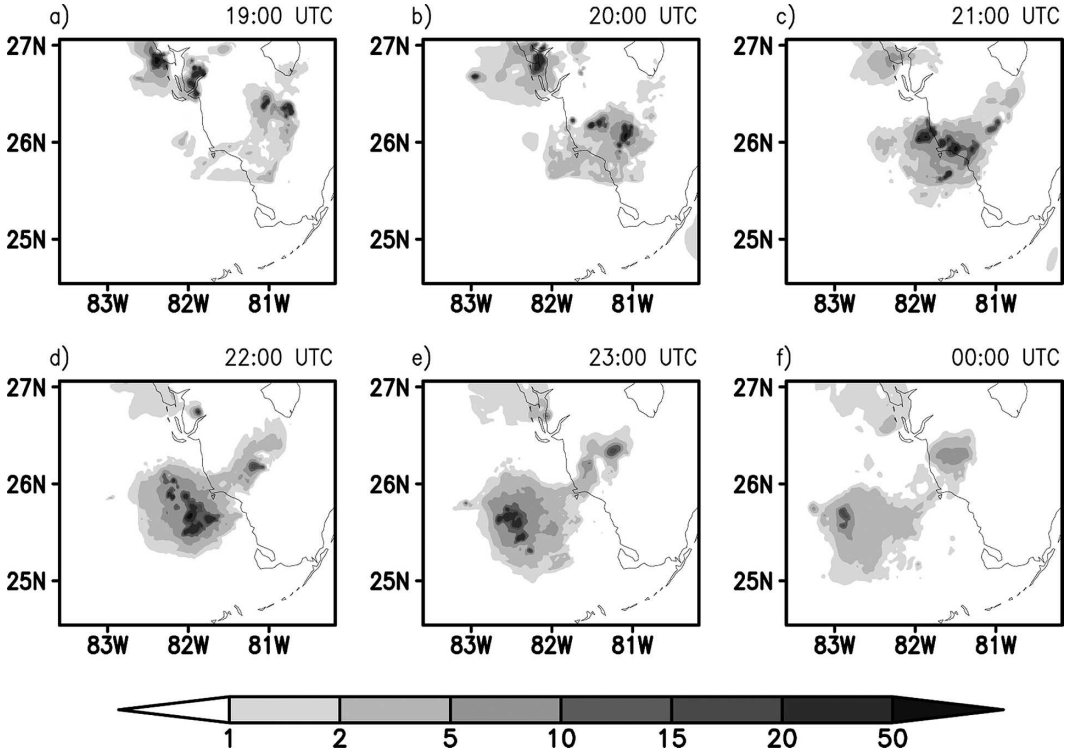

FIG. 5. Vertically integrated condensate (mm) at hourly intervals for the OBS simulation.

trations therefore decreases the spatial area of the anvil (on the order of 5%), but increases the amount of water mass in a vertical column, both of which will impact the radiative forcing of the anvil.

The convection in both simulations tends to move offshore more rapidly than was observed. This appears to be due to stronger cold pools in the simulations that overwhelm the sea breeze circulation more rapidly, thus allowing the convective cells to move off the coast earlier than in the observations. It should also be noted that the convection in the region of Fort Meyers (~26.5°N, 82°W) is not well-represented as this is beyond the northern grid boundary of grid 4. There is some redevelopment of the updrafts in the CLN case at 2300 UTC that does not occur in the OBS simulation or in the observations, again demonstrating that the latter case is more in keeping with observations.

The rest of the analysis will focus predominantly on the time period between 1800 and 2300 UTC, from when grid 4 is introduced to when the anvils start approaching the boundary of grid 3. Most of the results will be presented for grid 3 to provide a more overall view of the convective and anvil stages of development. The effects of grid 4 are, however, included in these results as the grid nesting is two-way interactive, although the magnitudes of some features may be less due to the grid cell averaging that occurs as information is passed up from grid 4 to grid 3.

b. *Updraft structure*

The development, structure, and west-to-southwestward progression of the updrafts for the CLN and OBS cases are evident in Fig. 6. It is apparent from this figure that the location of updraft development, the numbers of convective cores that develop, the strength of these cores, and the longevity of the updrafts differ between the two simulations. The updrafts are wider, stronger, and in closer proximity in the OBS case compared with those in the CLN simulation. To further investigate the updraft characteristics, the total number of updrafts at each vertical level in the CLN and OBS cases were binned using a 1 m s^{-1} bin width. The ratio of the number of OBS updrafts to the sum of the OBS and CLN updrafts was then calculated for each bin. The histograms in Fig. 7 show these ratios (expressed as a percentage) at ~3200 m AGL (low to midlevels) and at ~8700 m AGL (a level near which the maximum updrafts typically occur in both cases). This figure demonstrates that there are a greater number of stronger updrafts in the OBS case, until the development of the western convective core in the CLN case that was referred to earlier. Averaging the vertical velocities over

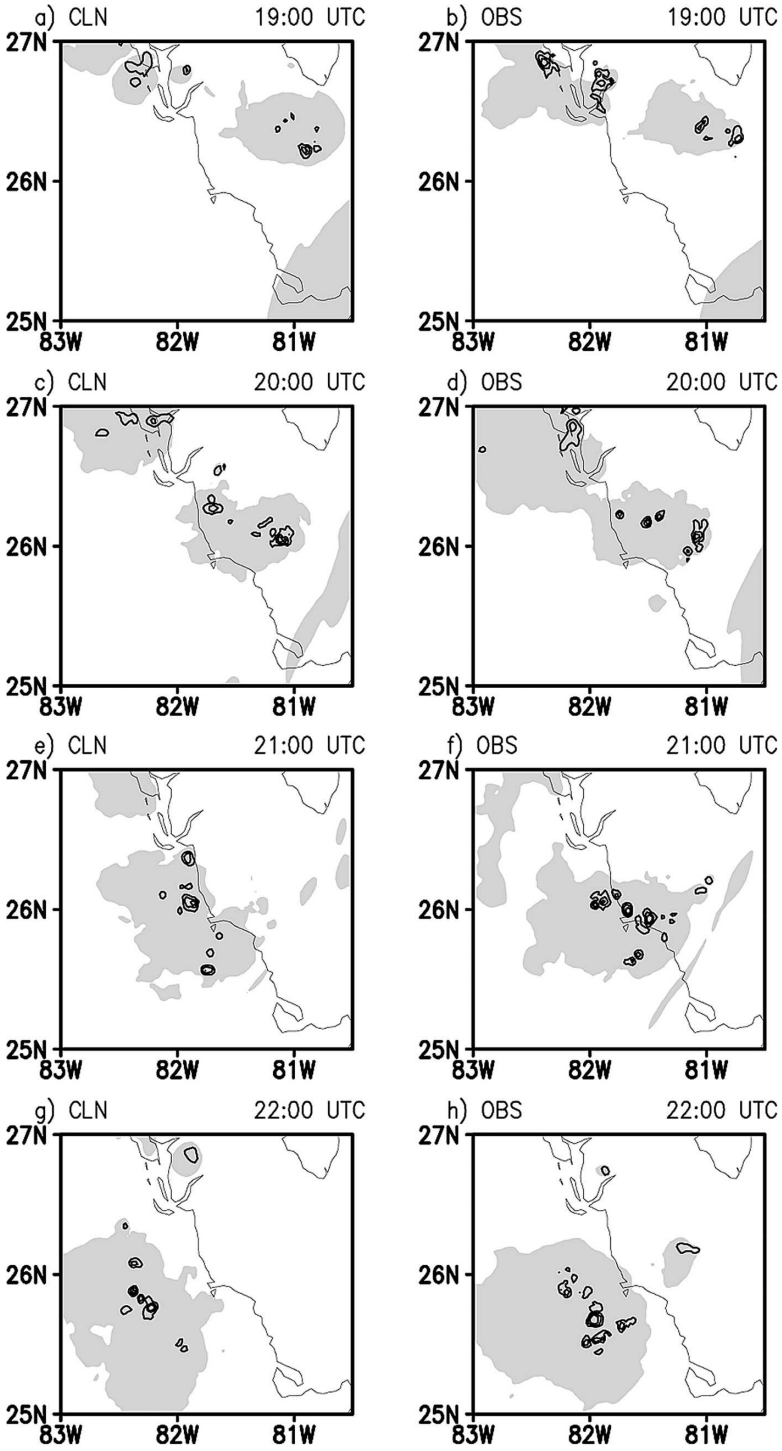

FIG. 6. The vertical velocity (lines, isolines at 1, 5, and 10 m s^{-1}) averaged between ~5500 and 13 700 m AGL and pristine ice + snow + aggregate mixing ratio (shading; mixing ratio values greater than 0.15 g kg^{-1} are shaded) for the (a), (c), (e), (g) CLN and (b), (d), (f), (h) OBS cases at hourly intervals from 1900 to 2200 UTC.

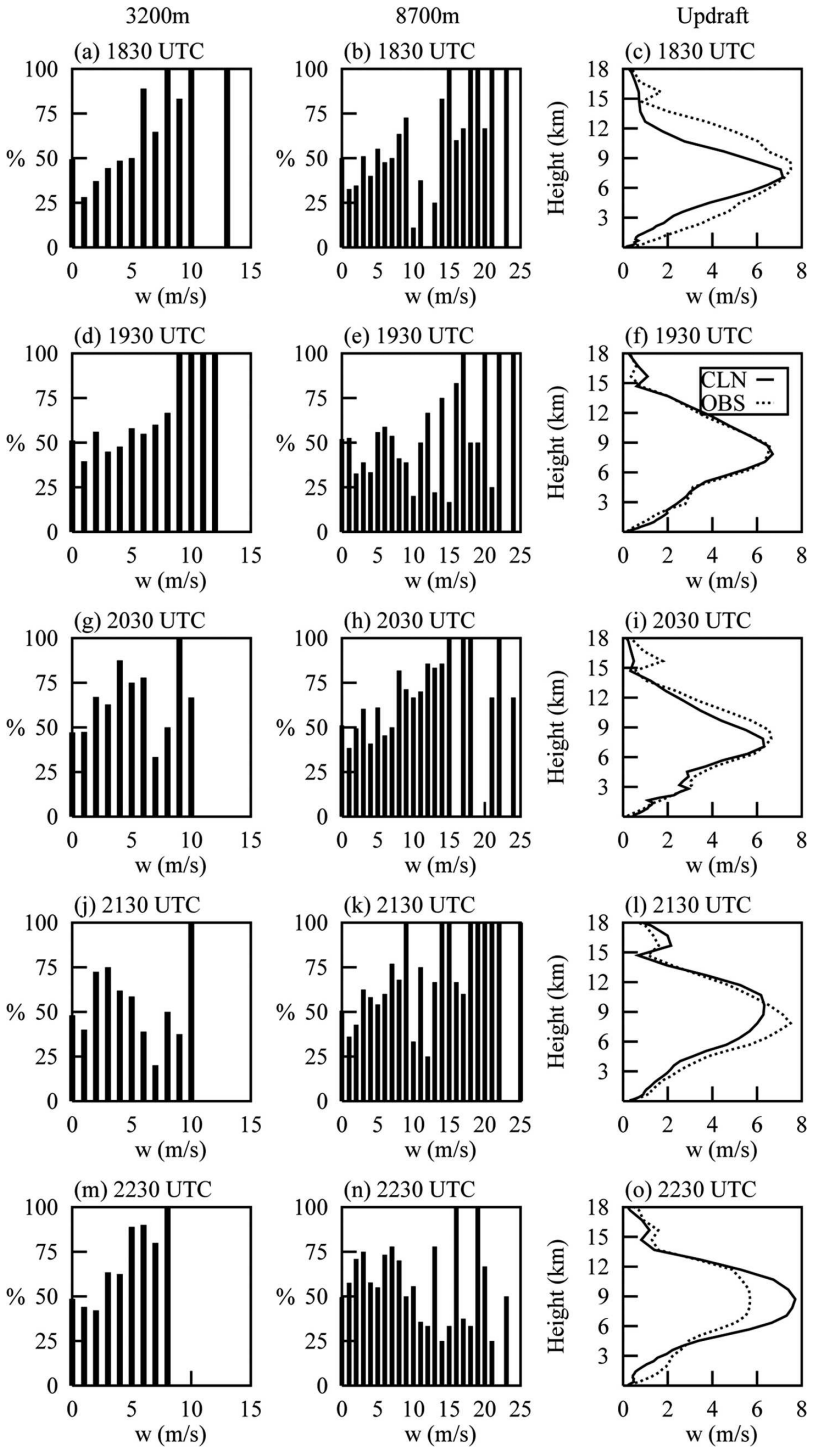

FIG. 7. Histogram of the number of updrafts in the OBS case to the sum of the number of updrafts in the CLN and OBS cases at (left column) ~3200 and (middle column) ~8700 m AGL, and (right column) horizontally averaged velocities within the updraft for the CLN (solid lines) and OBS (dotted lines) cases at hourly intervals starting at 1830 UTC.

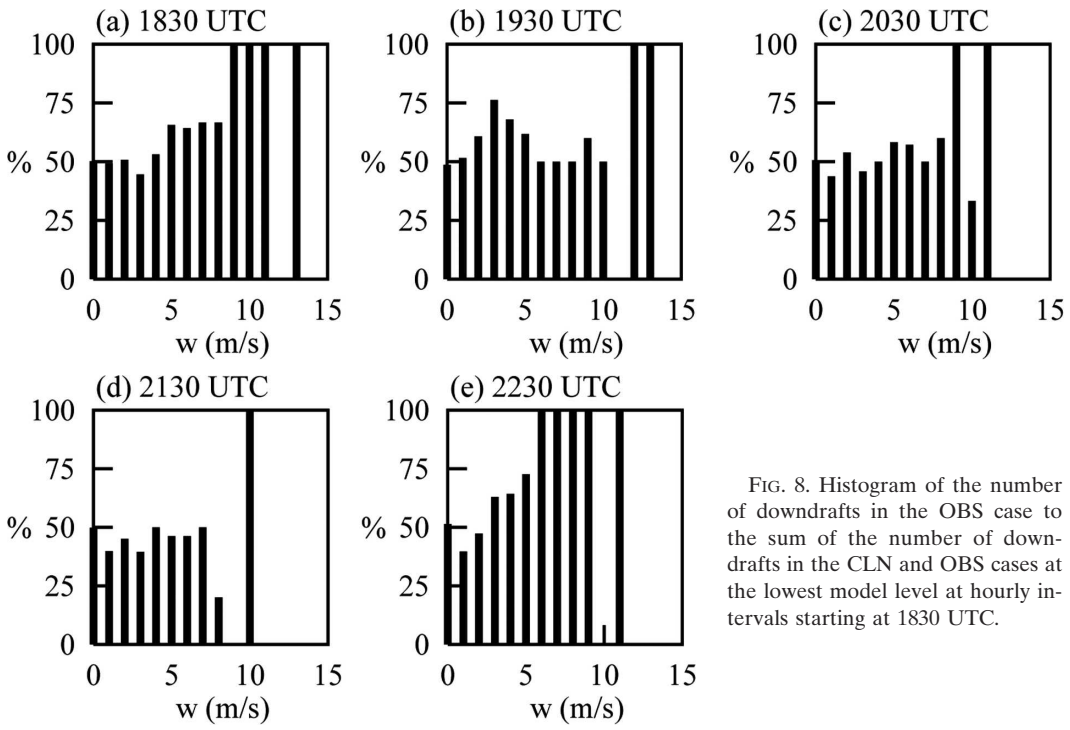

FIG. 8. Histogram of the number of downdrafts in the OBS case to the sum of the number of downdrafts in the CLN and OBS cases at the lowest model level at hourly intervals starting at 1830 UTC.

the convective cores (defined as the grid points where the vertical velocity averaged between 5700 and 14 700 m AGL is greater than or equal to 1 m s^{-1}) also demonstrate that the updrafts are stronger in the OBS case (Fig. 7, right column). The maximum updrafts occur between 8 and 10 km AGL for all sensitivity tests throughout most of the simulation and occur soon after 2000 UTC (not shown).

Radar-derived vertical velocities for 28 July 2002 were calculated utilizing the Eldora Doppler radar data obtained on board the P-3 aircraft using the methodology outlined in Straka (2004). The maximum radar-derived vertical velocity on 28 July was 32 m s^{-1}, whereas the strongest updraft in the OBS case study was 34 m s^{-1}. The observations thus support the vertical velocity magnitudes evident in the OBS simulation.

A plot similar to Fig. 7 was generated for the downdrafts at the lowest model surface (Fig. 8). It is apparent from Fig. 8 that enhancing the CCN, GCCN, and IFN concentrations results in a greater number of stronger downdrafts reaching the surface. A detailed analysis of the dynamic and thermodynamic characteristics of the updrafts and downdrafts is the focus of a paper currently in preparation for future publication.

Vertical profiles of the horizontally averaged vertical velocities for the sensitivity tests, represented as a difference between the sensitivity experiment and the CLN simulation, are shown in Fig. 9 for the initial (~1830 UTC), mature (~2030 UTC), and dissipating (~2230 UTC) stages of convection. During the initial stages of convective development, the updrafts in all the sensitivity tests are greater than those in the CLN case throughout most of the troposphere (Fig. 9a). This is due to the increase in the latent heat release associated with the formation of liquid and ice hydrometeor species on the increased number of aerosols. Focusing on the region where the maximum updrafts for all sensitivity tests occur (8–10 km AGL), those simulations involving increased concentrations of CCN appear to have the greatest impact on the initial updraft strength, with the simulations in which GCCN are enhanced being the least effective, and the impacts of increased IFN concentrations falling between these two extremes (Fig. 9a). It is interesting to note that differences between the CLN case and the sensitivity tests tend to be greater below and above the region of maximum updrafts during the initial storm stage, suggesting that variations in the aerosol concentrations may also play an important role in the vertical distribution of the updrafts.

During the mature stage of the convective core development the simulations with increased IFN concentrations have the greatest impact on updraft strength between 8 and 10 km, closely followed by those involving GCCN, while the impacts of CCN on updraft strength have been reduced (Fig. 9b). The sensitivity test in which only the concentrations of CCN are en-

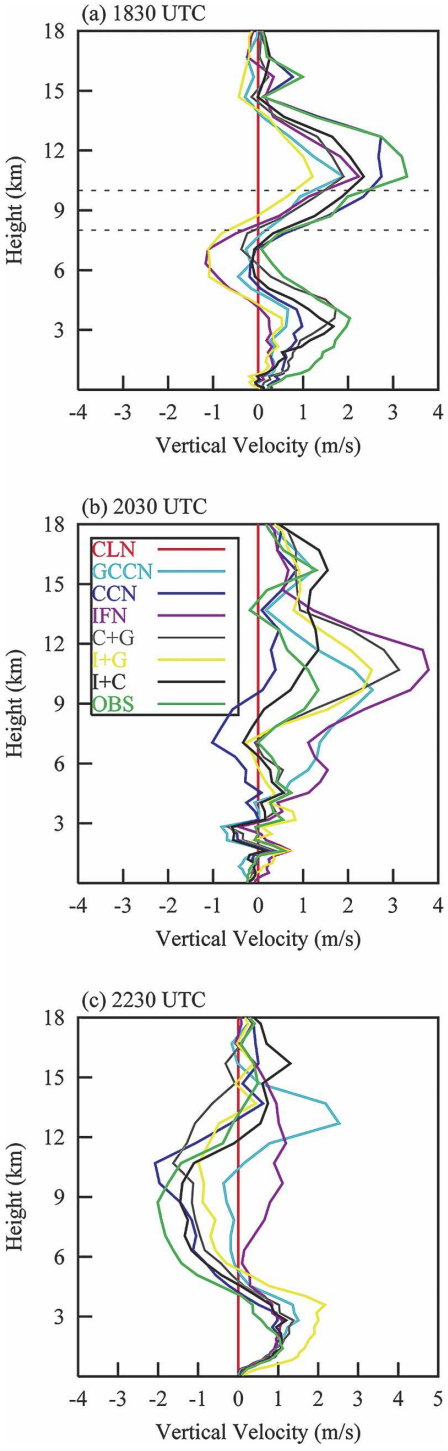

FIG. 9. Vertical profiles of the difference of the sensitivity experiments and the CLN case for the horizontally averaged vertical velocity within the convective cores (defined to be the regions where the updrafts are greater than or equal to 1 m s^{-1}) for (a) the initial stage in convective development, (b) the mature stage of convective development, and (c) the dissipating stage of convective development. The sensitivity experiments may be identified using the key in (b). The two horizontal dotted lines shown in (a) indicate the region in which the maximum vertical velocities fall for all sensitivity tests between 1800 and 0000 UTC.

hanced actually reduces the updraft strength when compared with the CLN case. Then, as the convective cores start to weaken, all the sensitivity tests, with the exception of the IFN test, reveal updrafts weaker than those in the CLN case (Fig. 9c).

A vertical cross section through the updraft maxima at 1900 UTC for the CLN and OBS cases (Fig. 10) demonstrates significantly greater amounts of the second cloud water mode (which is nucleated by GCCN) within the updraft. Between 5 and 7 km AGL, the cloud water mixing ratios in the OBS simulation are as much as 40 times greater than those in the CLN case. The greater latent heat release associated with the higher cloud water mixing ratios in the OBS case contributes to the development of the stronger updrafts in the OBS simulation compared with those in the CLN case. This is also true for the GCCN simulation (not shown). The loss of GCCN as a result of the formation of the cloud water is also apparent, especially in the lower regions of the updraft.

These vertical velocity results demonstrate several important points. Simply increasing aerosol concentrations can have a 3–4 m s^{-1} increase on the horizontally averaged updraft strength, a significant effect given that these are horizontal averages and not maximum quantities, and that the largest horizontally averaged updrafts are on the order of 8 m s^{-1}. Variations in aerosol concentrations therefore not only affect microphysical properties, but also have the potential to change the dynamics of the entire storm system. Previous research has focused primarily on how increases in CCN number concentrations tend to reduce warm rain efficiencies and increase cloud water contents (e.g., Warner and Twomey 1967; Albrecht 1989; Kaufman and Nakajima 1993; Borys et al. 1998; Rosenfeld 1999, 2000; Andreae et al. 2004). Greater amounts of liquid water are thus available to be transported vertically, which provides greater amounts of supercooled water that can freeze, the release of greater amounts of latent heat, and subsequent increases in updraft strength. While this is found in these simulations, the sensitivity tests indicate that enhanced GCCN and IFN concentrations have a more significant impact on updraft strength during the mature and dissipating stages of convection, and that the effects of enhanced CCN concentrations are only dominant during the initial stages of convective development. We know from previous modeling studies that the rapidity of glaciation is greater in the presence of supercooled raindrops (Cotton 1972; Koenig and Murray 1976; Scott and Hobbs 1977). Later in the storm's life cycles, rain is more prevalent and thus enhanced concentrations of IFN will result in rapid glaciation of the convective towers. Moreover, the presence of

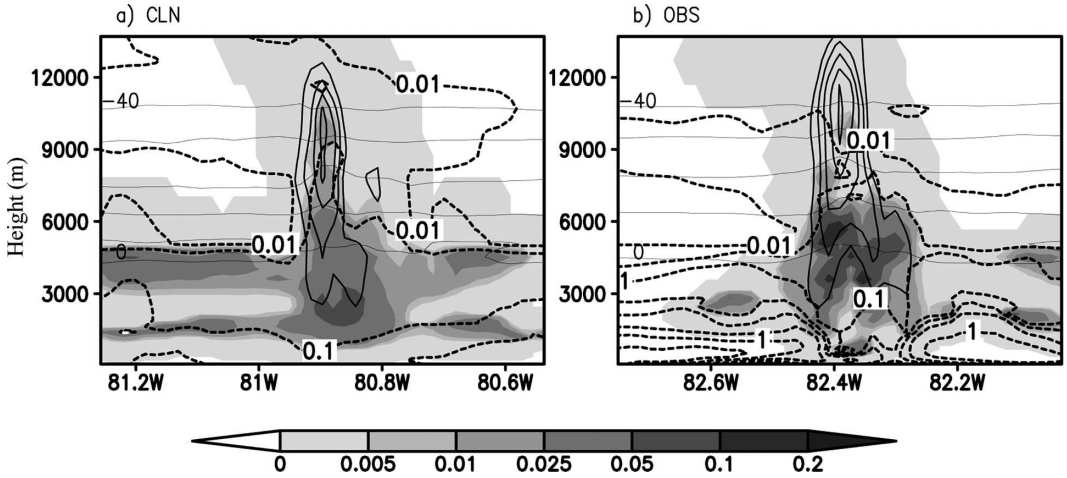

FIG. 10. Vertical cross sections through the updraft core at 1900 UTC for the (a) CLN and (b) OBS cases. Dotted lines represent GCCN number concentrations (0.01, 0.05, 0.1, 0.2, 0.3, 0.5, and 1 cc^{-1} isolines are shown), shading represents the second cloud water mode mixing ratios (g kg^{-1}), solid lines represent vertical velocity (5 m s^{-1} contour interval), and solid horizontal lines are isotherms from 0° to −40°C at 10°C intervals.

GCCN will enhance rain formation, thereby favoring rapid and complete glaciation of the convective towers.

c. *Microphysical impacts*

Vertical profiles of the horizontal averages of the liquid water and ice hydrometeors within the convective updrafts are shown in Figs. 11 and 12, respectively. Comparing the cloud water mixing ratios for the CLN and OBS cases (left column of Fig. 11) demonstrates that the cloud water mass is greater in the OBS case throughout the simulation due to the presence of the enhanced aerosol concentrations. Cloud water does extend above the freezing level (~5 km AGL) in both cases, thus providing supercooled liquid water for collision and riming processes. Between 1800 and ~2000 UTC, the rain mixing ratios are less in the OBS case; however, by 2030 UTC those in the OBS case are greater (right column of Fig. 11). This demonstrates the delay in rain formation associated with enhanced aerosol concentrations, narrower cloud droplet distributions, and reduced collision efficiencies.

The mass of pristine ice + snow is greatest in the OBS case, and the anvils are also consistently deeper in this case (left column of Fig. 12) compared with the CLN simulation. Both of these aspects have significant impacts on the cloud radiative forcing by the anvil. Pristine ice and snow mixing ratios are larger in the OBS case due to the higher IFN concentrations, which enhance heterogeneous nucleation. The greater amounts of supercooled liquid water in this case also facilitate the homogeneous freezing of pristine ice and the riming of snow flakes, both of which will increase the ice mass.

Aggregate mixing ratio maxima are typically larger throughout the simulation in the CLN case (second column of Fig. 12), although the vertical extent through which they occur does tend to be greater in the OBS case. In the CLN case, lower IFN number concentrations mean reduced competition for vapor and supercooled water, a wider size distribution and a more efficient collection process of pristine ice, snow, and other aggregates by aggregates themselves. The location of the aggregates maxima does tend to shift in the vertical given that aggregates have relatively significant fall speeds.

The graupel mass maxima are greatest, throughout most of the time period of interest, in the CLN case (third column of Fig. 12), whereas hail mixing ratios are larger in the OBS simulation (fourth column in Fig. 12). The hail variable in RAMS represents high-density frozen raindrops or hailstones. Like aggregates, both hail and graupel occur throughout a deeper layer in the OBS case. In the OBS case, larger amounts of available cloud water enhance riming rates. Graupel, as defined in RAMS, can only withstand a modest amount of riming, after which it is transferred to the hail category. The greater LWCs and associated riming in the OBS case therefore result in more graupel being transferred to the hail category. This is seen more clearly below.

Vertical profiles of the horizontally and temporally (1800–0000 UTC) averaged liquid water and ice species within the updraft, represented as a difference between the sensitivity test and the CLN case, are shown in Fig. 13. Between ~2 and 5 km AGL, enhancement of all three aerosol species generally results in greater

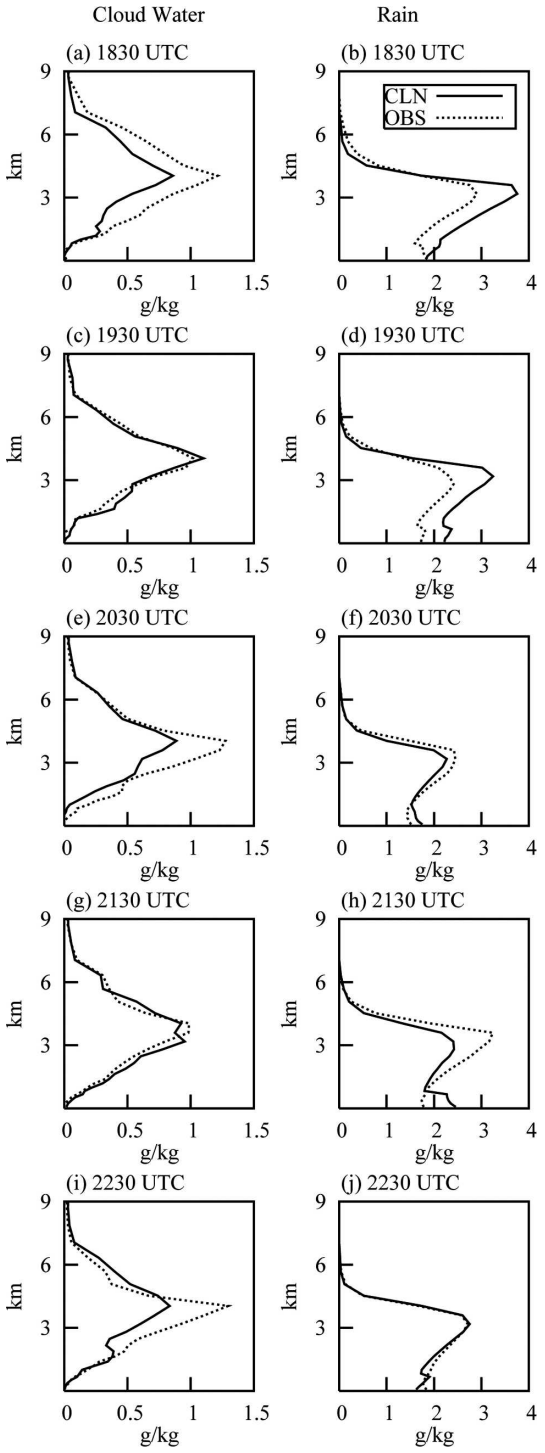

FIG. 11. Horizontally averaged (left column) cloud and (right column) rain mixing ratios at hourly intervals starting at 1830 UTC for the CLN (solid line) and OBS (dotted line) cases.

amounts of cloud water being produced compared with the CLN case (Fig. 13a). The sole enhancement of GCCN produces the most cloud water, followed by the case in which both CCN and GCCN concentrations are simultaneously increased. The high cloud water mixing ratios in the IFN case occur as a result of the melting of the ice species such as ice crystals and aggregates. The melting level is at ~5 km AGL.

It is apparent from Fig. 13b that independently enhancing IFN or GCCN concentrations produces the greatest amount of rainwater at the surface, through melting processes in the former case, and through increased collection processes associated with a wider droplet size distribution in the latter. More rainwater is also produced at the surface in the OBS case compared with that in the CLN case. All of the cases in which the CCN concentrations were enhanced, with the exception of the OBS case, produced less rainfall at the surface compared with the CLN case. The low rain mixing ratios in the CCN sensitivity test supports previous findings regarding the impacts of CCN on warm rain production (e.g., Warner and Twomey 1967; Albrecht 1989; Kaufman and Nakajima 1993; Borys et al. 1998; Rosenfeld 1999, 2000; Andreae et al. 2004). Simultaneously increasing the GCCN and CCN concentrations resulted in more rainfall at the surface than when CCN concentrations are simply increased, thus demonstrating the role of GCCN in rain production at the surface. A similar result holds true for IFN. Enhancing the concentrations of CCN and GCCN simultaneously does, however, produce less rainfall at the surface than the CLN case. This is somewhat surprising in that a wider size distribution could be expected to produce raindrops more efficiently. However, as it will be demonstrated below, the GCCN are depleted relatively quickly, and the effects of the enhanced CCN then dominate.

Between ~9.5 and 11 km AGL, increases in IFN concentrations produce the same ice crystal mixing ratios as the rest of aerosol enhancements produce higher up (Fig. 13c), supporting previous observations that the presence of Saharan dust allows for ice nucleation at warmer temperatures (Schaefer 1949, 1954; Isono et al. 1959; DeMott et al. 2003; Sassen et al. 2003). The anvil is also deeper in this case. Higher up, however, the simultaneous enhancement of CCN and GCCN concentrations produces the greatest differences from the CLN case. The enhancement of both CCN and GCCN produces large amounts of cloud water but relatively little rain, which means that relatively high LWCs are available for ice formation. Also, in the IFN case, which also produces high cloud water contents, the formation of ice at warmer temperatures deprives the upper levels of available moisture. All of the sensitivity tests produce greater amounts of ice compared with the CLN case because of the greater amounts of liquid water available for freezing.

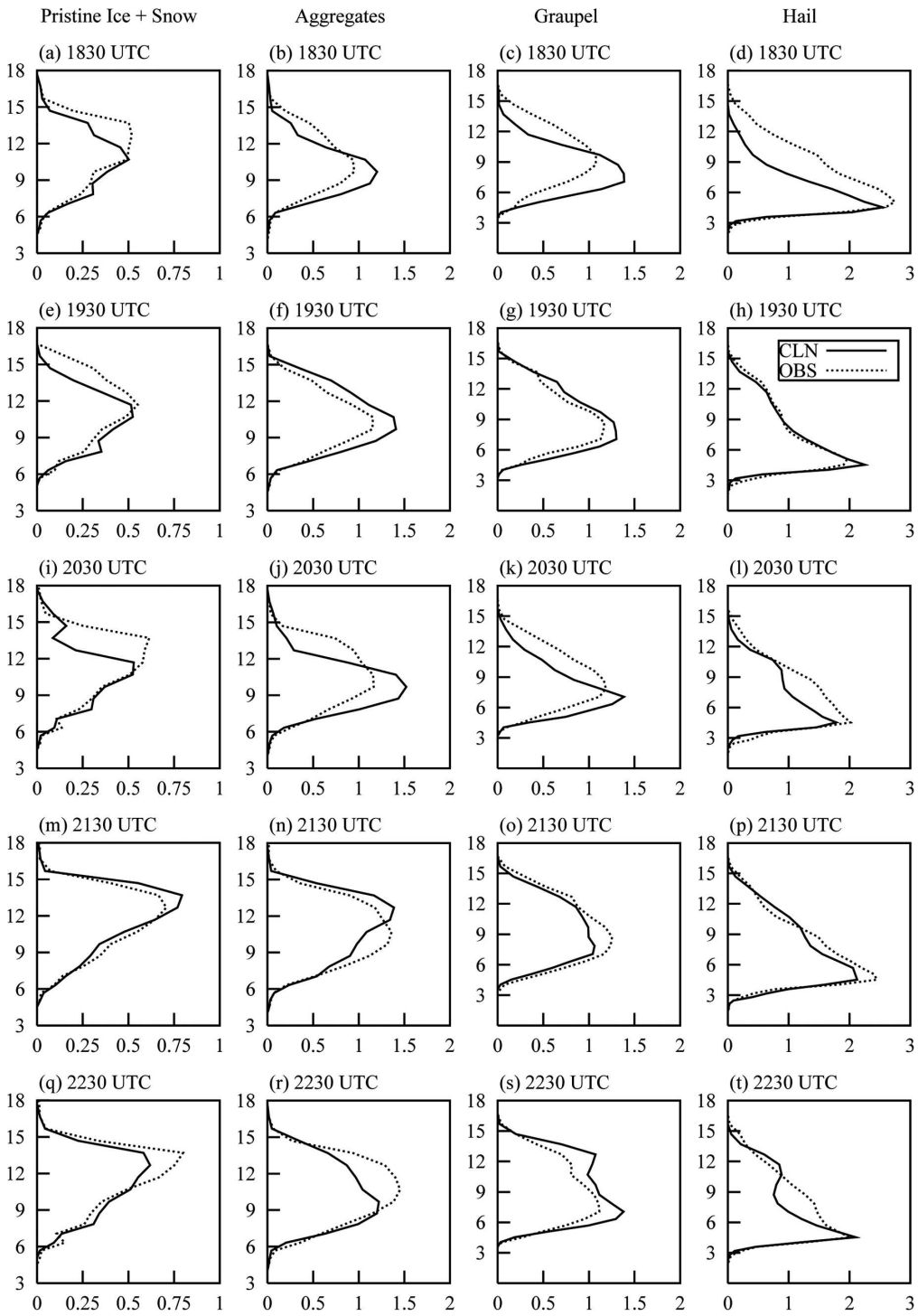

FIG. 12. Horizontally averaged (left column) ice + snow, (second column) aggregates, (third column) graupel, and (right column) hail mixing ratios at hourly intervals starting at 1830 UTC for the CLN (solid line) and OBS (dotted line) cases. The abscissa is mixing ratio (g kg^{-1}) and the ordinate is height (km).

Below ~9 km AGL, all of the sensitivity tests result in a reduction in graupel compared with the CLN case, with those in which CCN concentrations are enhanced having the greatest effect (Fig. 13e). As the melting level (~5 km AGL) is approached, the differences between the simulations become insignificant. The trends in the hail mixing ratio differences below 9 km AGL are almost a mirror image of those of graupel, with

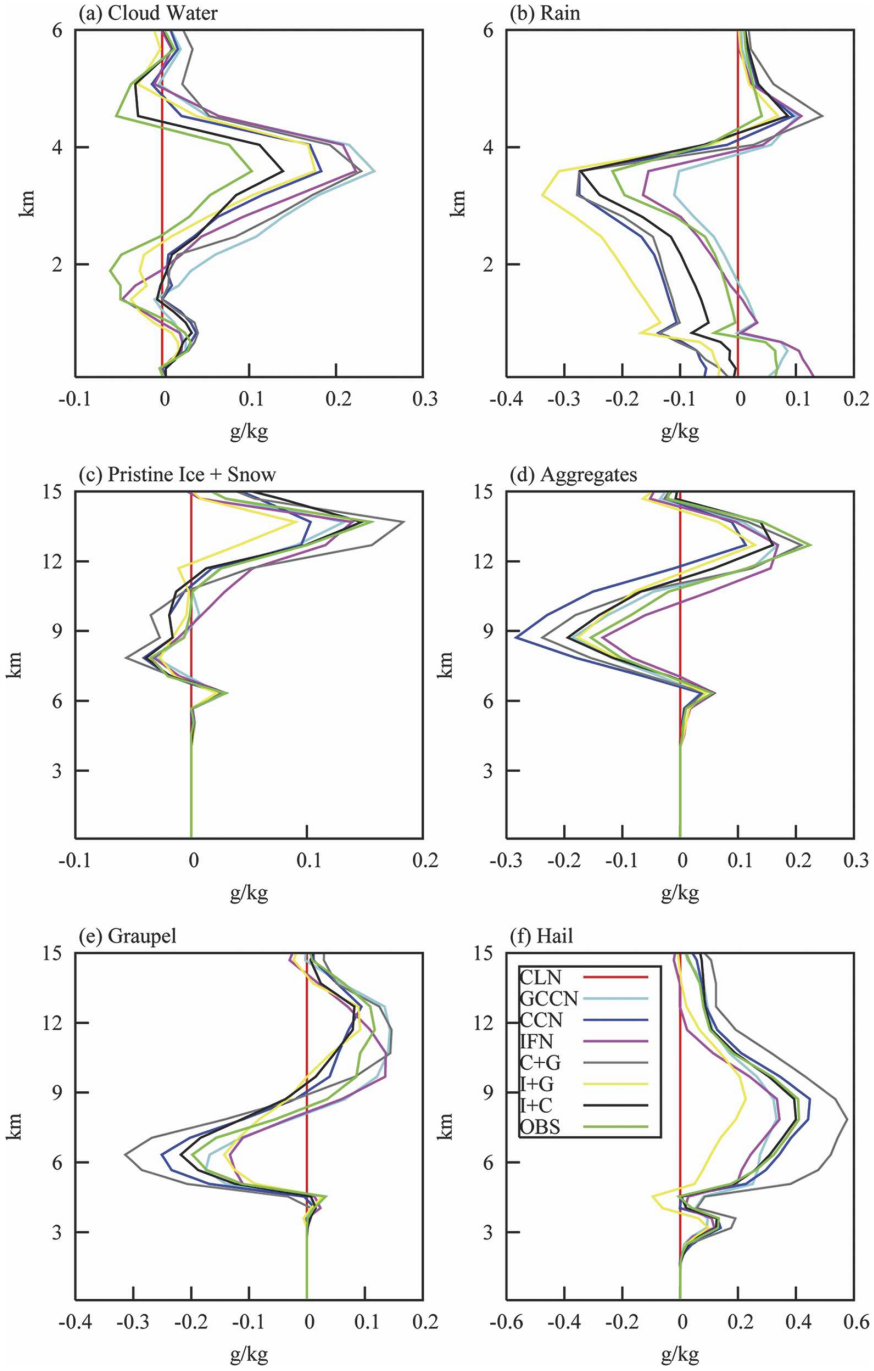

FIG. 13. Vertical profiles of the difference between the sensitivity tests and the CLN simulation (red) for the horizontally and temporally (1800–0000 UTC) averaged (a) cloud water, (b) rain, (c) pristine ice + snow, (d) aggregates, (e) graupel, and (f) hail mixing ratios within the updrafts. The profiles of the sensitivity tests are labeled in the key in (f).

most hail being produced when CCN and GCCN are simultaneously enhanced. In this case, large amounts of cloud water are produced that will enhance the riming of graupel, and force these hydrometeors into the hail category in which the hydrometeors are larger and may contain a greater percentage of liquid water on their surface. As hail is also formed by the freezing of raindrops, the large rain mixing ratios in the C + G case between 4 and 6 km AGL provide a major source for hail formation in this region. Preliminary investigations

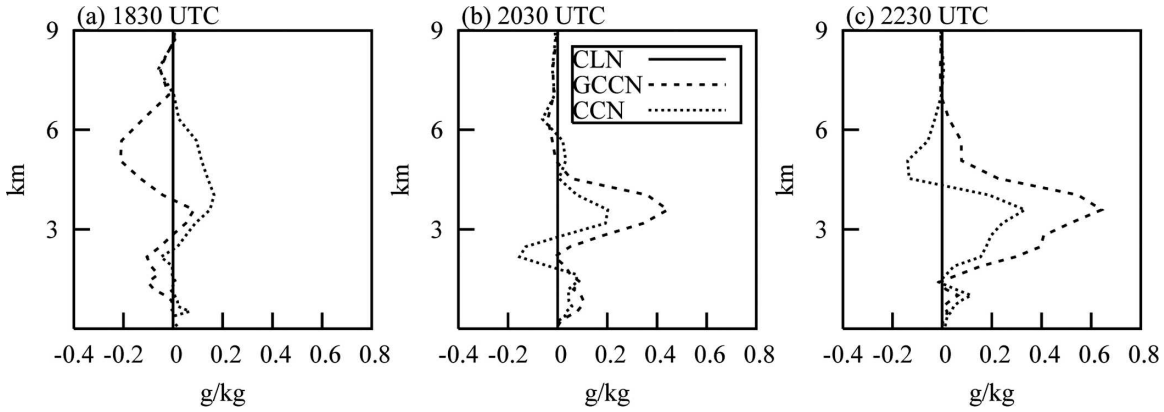

FIG. 14. Vertical profiles of the difference between the GCCN and CCN sensitivity experiments and the CLN case for the horizontally averaged cloud water mixing ratios within the convective cores for (a) the initial stage in convective development, (b) the mature stage of convective development, and (c) the dissipating stage of convective development. The sensitivity experiments may be identified using the key in (b).

into the effects of Saharan dust on hail in France suggest that there is a large deficit in smaller hailstones (diameters <1.4 cm) in the presence of Saharan dust (Dessens et al. 2004). That the graupel mass is reduced and the hail mass is increased in our simulations for all the dust cases compared with the CLN case lends some support to their findings.

The differences in vertical velocity and cloud water due to variations in aerosol concentrations suggest a possible microphysical–dynamical feedback mechanism. It was seen above that the enhanced GCCN case produces higher time-averaged cloud water mixing ratios than the enhanced CCN case (Fig. 13a). Examining the cloud water field at specific times demonstrates that during the initial stages of the storm, the enhanced CCN case produces more cloud water than the enhanced GCCN case, but this trend reverses during the mature and dissipating stages (Fig. 14). A similar reversal was also seen for the vertical velocity field (Fig. 9) in that updrafts were stronger in the enhanced CCN case initially, but during the mature and dissipating stages the updrafts were stronger in the enhanced GCCN case. The following hypothesis is put forward: initially greater amounts of cloud water are produced in the enhanced CCN experiment, the contributions of which come primarily from the first cloud mode. The associated release of latent heat produces the stronger updrafts. However, as the simulations progress and cloud water is transported vertically, the second mode of cloud water associated with GCCN becomes more important as this mode is more effective in ice phase interactions; for example, larger droplets are more effectively collected by ice particles, and larger droplets undergo homogeneous freezing more rapidly. In the GCCN case, greater amounts of the second cloud water mode are produced, and hence the associated release of latent heat upon interacting with ice is greater. This results in the stronger updrafts in the GCCN case during the mature and dissipating stages. Stronger updrafts (in all cases) result in the more rapid production of cloud water and pristine ice, which in turn enhances the updraft strengths, and so the feedback cycle continues. This hypothesis is being investigated in more detail in a paper currently being written that includes a detailed investigation into precipitation and anvil efficiencies, and the energy fluxes within these storms systems.

Examining a time series of the contributions of cloud water to the total liquid water mass (Fig. 15a) demonstrates that the cloud water fraction is greatest between 2000 and 2100 UTC, during the development of the strongest updrafts. The GCCN case initially has the greatest cloud water fraction, while the rain contribution is greatest in the CLN case in the first couple of hours, representing a more efficient warm rain process in this case. The CCN case undergoes the least variation in the cloud water contribution and has the greatest cloud water contributions at the end of the simulation, being the least effective sensitivity test in converting cloud water to rain. These ratios support the trends observed in the temporally and spatially averaged cloud water and rain mixing ratios shown in Fig. 13.

A time series of the contributions of liquid water to the total condensate, shown in Fig. 15b, reveals that the CLN case has the greatest liquid water contributions. The cases in which two or more of the aerosol species were enhanced have the least liquid water contributions, supporting the fact that under dirty or dusty conditions, more liquid water is transferred vertically and is available for ice formation. The GCCN case has the second largest liquid water contribution

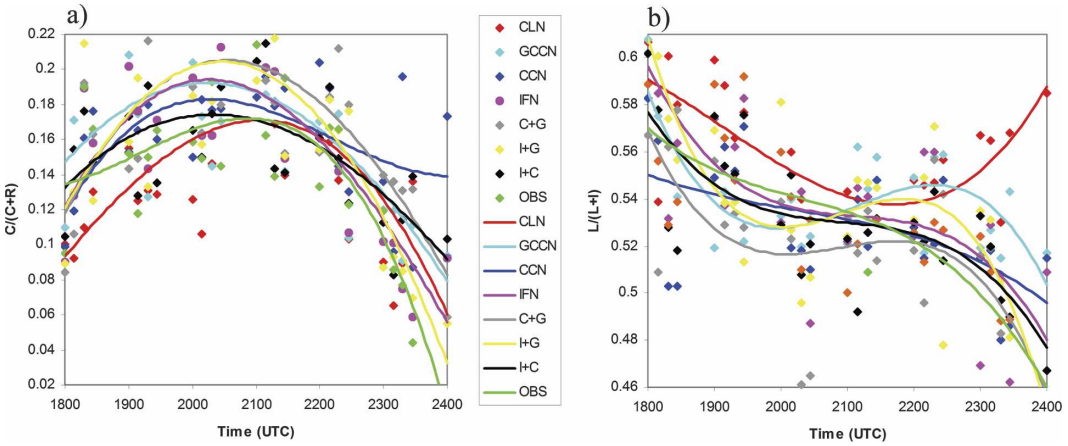

FIG. 15. Scatterplot of the ratio of (a) vertically integrated cloud water/vertically integrated (cloud water + rain) mixing ratios and (b) vertically integrated liquid/vertically integrated (liquid + ice) mixing ratios, as a function of time for all the sensitivity experiments within the updrafts. Lines represent the best third-order polynomial fit [R^2 values range from 0.48 to 0.8 in (a) and from 0.5 to 0.7 in (b)].

after the CLN case from 2100 UTC onward, which corresponds to the greater cloud water and rain mixing ratios found in this case compared with the other sensitivity tests.

d. Accumulated surface precipitation

Another aspect associated with convective storms that is affected by variations in aerosol concentrations is the accumulated surface precipitation. The accumulated surface precipitation for the entire area of grid 3 for each of the sensitivity tests is shown in Table 4. It is apparent that by 1800 UTC, most surface precipitation has occurred in the cases in which IFN and GCCN concentrations are enhanced, followed by the case in which IFN and GCCN concentrations are increased simultaneously. All three of these cases produce more surface precipitation than in the CLN experiment. All of the sensitivity tests in which CCN concentrations were enhanced result in a decrease in the surface precipitation at this time.

The dominance of the sensitivity tests in which IFN and GCCN concentrations are increased suggest a response similar to dynamic seeding concepts in which enhanced glaciation of convective clouds leads to dynamical invigoration of the clouds, larger amounts of processed water, and thereby enhanced rainfall at the ground (Simpson et al. 1967; Rosenfeld and Woodley 1989, 1993) By 0000 UTC, the total surface precipitation is greatest in the CLN case, demonstrating the reduction in surface precipitation associated with the increases in aerosol concentrations. Of the dirty cases, increases in GCCN concentrations results in the most surface precipitation, followed by the enhancements of IFN. All the simulations involving CCN produce the least surface precipitation, even less than the observed case.

TABLE 4. Accumulated surface precipitation (acre–feet) for the eight sensitivity tests described in the text, in descending order, and the factors from the factor analysis, also in descending order, at 1800 and 0000 UTC.

1800 UTC				0000 UTC			
Accumulated precipitation		Factor separation		Accumulated precipitation		Factor separation	
Exp Name	Magnitude	Factor name	Magnitude	Exp name	Magnitude	Factor name	Magnitude
IFN	66 608	f_0 (CLN)	63 289	CLN	442 168	f_0 (CLN)	442 618
GCCN	65 874	f_{123} (I + C + G)	8479	GCCN	368 053	f_{12} (I + C)	79 066
I + G	63 487	f_1 (IFN)	3318	I + G	352 112	f_{13} (I + G)	76 852
CLN	63 289	f_3 (GCCN)	2584	IFN	349 373	f_{23} (C + G)	57 335
CCN	61 741	f_2 (CCN)	−1548	OBS	346 309	f_{123} (I + C + G)	−44 375
C + G	58 275	f_{13} (I + G)	−5705	CCN	344 338	f_3 (GCCN)	−74 114
I + C	57 700	f_{23} (C + G)	−6050	I + C	330 610	f_1 (IFN)	−92 794
OBS	57 008	f_{12} (I + C)	−7359	C + G	327 560	f_2 (CCN)	−97 829

The factor separation technique (Stein and Alpert 1993) was used to isolate the effects of each aerosol (f_1, f_2, f_3) as well as the effects of the interactions between the aerosols (f_{12}, f_{13}, f_{23}, f_{123}) on the accumulated surface precipitation when compared with the CLN case. It should be noted here that the interactions between the aerosols refers to the effects of the actual interactions between the various aerosol species, and not the total output in which the concentrations of two or more aerosol concentrations are enhanced. For example, the factor f_{13} demonstrates the impact that the interactions between GCCN and IFN have on total precipitation by subtracting out the impacts that GCCN and IFN have independently on the final output. The factor f_{13} should not therefore be confused with the total precipitation produced in I + G. The factor separation technique demonstrates that while the IFN and GCCN enhancements contribute to the total surface rainfall at 1800 UTC, the impacts of the CCN, as well as the actual interactions between any of the two aerosol species, are detrimental to surface precipitation production. Interestingly, the interactions between all three species (f_{123}) enhance surface rainfall at this time when compared with the CLN case. By 0000 UTC, the interactions between any two aerosol species enhance surface precipitation, whereas increases in each of the three aerosol species reduces surface precipitation when compared with the CLN case.

It is somewhat surprising that the CLN case produces more surface precipitation compared with the GCCN sensitivity test, given that the introduction of GCCN tend to widen the droplet spectrum and enhance the collision–coalescence process. This may in part be attributed to the rapid depletion of GCCN through several different processes. In Fig. 16 it is evident that the initial updraft development to the south of Lake Okeechobee occurs in regions that are rich in GCCN in the lower levels compared with that in the CLN case. Two hours later though, the updrafts in the CLN and GCCN cases are located within environmental air that have similar GCCN concentrations. In the GCCN case, GCCN concentrations are relatively low over the ocean where high relative humidities result in the formation of low-level clouds, and over land in association with the sea breeze frontal passage (see Fig. 2) which provides sufficient lift to nucleate droplets in the second cloud water, both of which deplete GCCN.

Finally, it must be emphasized that the accumulated surface precipitation totals just discussed were for the entire area of grid 3 and thus include the precipitation produced by ordinary cumulus also observed on this day (see Fig. 2), as well as the precipitation processes associated with the sea breeze convection, the frontal passage and the low-level clouds that develop over the western regions of the peninsula. All of these systems affect and are affected by variations in aerosol concentrations. The trends in the accumulated precipitation over the entire grid do differ from those trends in the surface rainfall observed above. This highlights the fact that a complex set of interactions and water sources and sinks may occur throughout a large region as a result of natural (or anthropogenic) seeding.

4. Discussion and conclusions

The results of the simulations presented in this paper, which were performed to investigate the sensitivity of Florida convection to variations in the concentrations of nucleating aerosol, demonstrate that variations in aerosol concentrations have a significant impact on both microphysical and dynamical characteristics of convective storms over the Florida Peninsula, as well as on the accumulated surface precipitation. While the variations in microphysical characteristics would typically be expected, significant changes to the storm dynamics may not be so. It is apparent from these results that the whole dynamical structure of the storm can be influenced by simply varying the concentrations of cloud-nucleating aerosol. In particular, the updrafts are consistently stronger and more numerous in the OBS case when compared with the CLN case, being driven by the latent heat release due to freezing of larger amounts of supercooled water associated with higher aerosol concentrations within the storm. While the variations in the strength of the updrafts have previously been linked to changes in CCN concentrations with less attention being given to GCCN and IFN, it is demonstrated here that CCN have the greatest impact on updraft strength during the initial stages, whereas GCCN and IFN concentrations have a greater impact on updraft strength during the mature and dissipating storm stages.

The particular microphysical characteristics affected by variations in aerosol concentrations include greater anvil area coverage in the CLN case, but the anvil in the OBS case is better-organized and contains much greater condensate maxima. Cloud water increases with increasing aerosol concentrations, with increases in GCCN concentrations producing the most cloud water on average. Surface rainfall is greatest when GCCN or IFN concentrations are enhanced. Increasing CCN concentrations reduces the surface rainfall compared with the CLN case, while simultaneously enhancing CCN and GCCN does produce more rain than when only CCN are enhanced. Increasing IFN concentrations re-

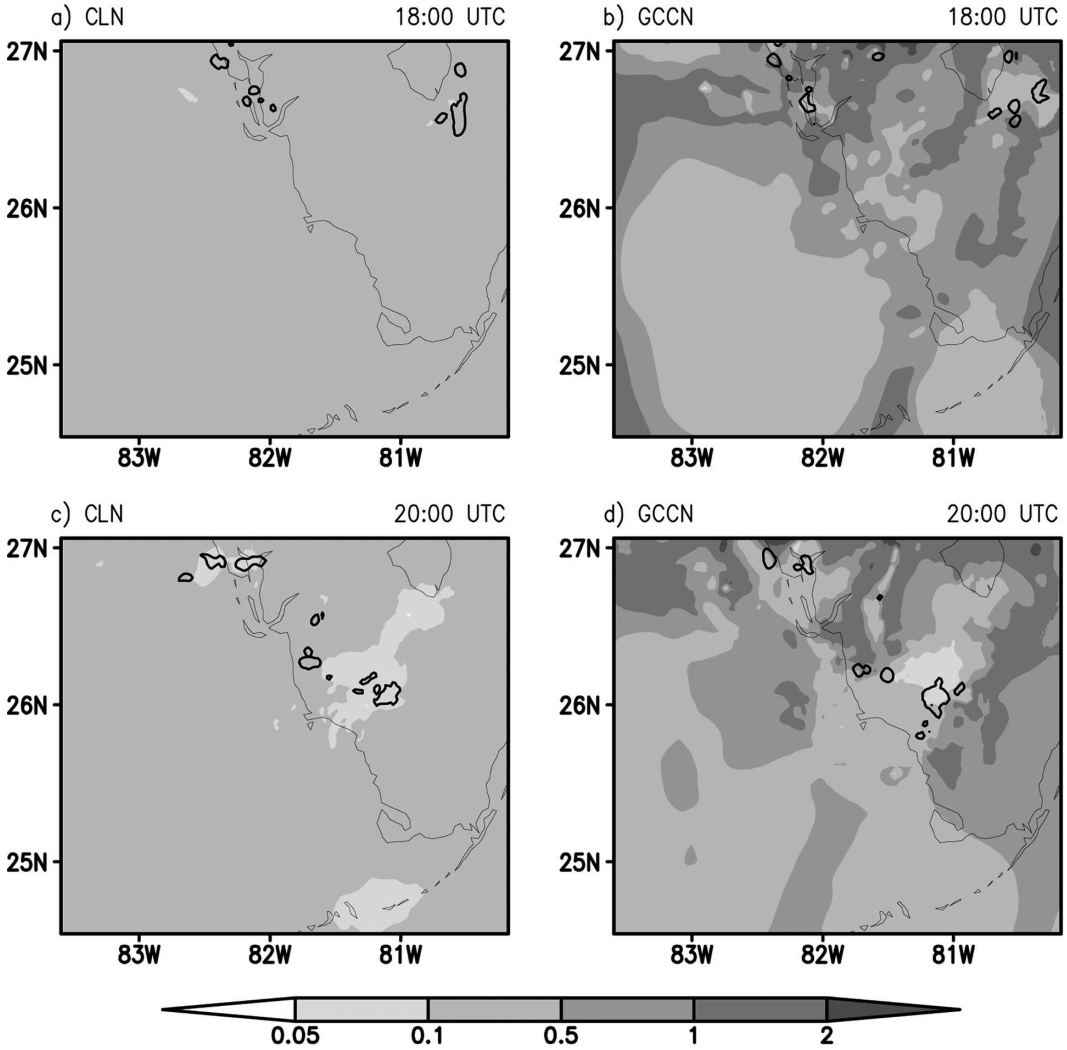

FIG. 16. GCCN concentrations (shaded; cm^{-3}) at 1 km AGL and the updraft cores averaged between 5700 and 14 700 m AGL (solid lines; only the 1 $m\ s^{-1}$ isoline is shown) for the (a), (c) CLN and (b), (d) OBS cases at (a), (b) 1800 and (c), (d) 2000 UTC.

sults in the formation of ice particles at warmer temperatures and a deeper anvil, however, the greatest anvil ice mixing ratios occur in the C + G case due to the high LWCs and the fact that ice begins nucleating at lower levels in the IFN case, thus depriving higher levels of liquid water and vapor. In general, graupel mixing ratios are reduced while hail mixing ratios are increased when aerosol concentrations are increased. This appears to be due to the transfer of graupel to the hail category as the graupel riming rates increase with increased aerosol concentrations.

The contribution of cloud water to the total liquid water is greatest in the CCN case, demonstrating the inefficiency of converting cloud water to rain when CCN concentrations are high, whereas in the CLN case, the cloud water contribution is relatively low demonstrating a more effective warm rain process. Also, as the aerosol concentrations are increased, so the relative contributions of ice to the total condensate mixing ratios are increased. This occurs as more cloud water is available with increases in aerosol concentrations, the warm rain process is inhibited, and more liquid water is transported upward where it is available for freezing and riming.

The accumulated surface precipitation is initially greater in the cases in which the GCCN and/or IFN concentrations are enhanced than in the CLN run. However, at the end of the simulation, while enhancements in both GCCN and IFN still produce more precipitation at the surface than when CCN concentrations are increased, the accumulated precipitation is greatest in the CLN case, demonstrating the reduction in sur-

face precipitation associated with increases in aerosol concentrations.

Based on the results of their modeling study of storms that developed during CRYSTAL–FACE, Fridland et al. (2004) advanced the hypothesis that aerosols between 6 and 10 km had the greatest impact on the cirrus anvil microphysics. However, the simulations presented here demonstrate that many characteristics of both the convective and anvil stages of storm development are sensitive to changes in the aerosol concentrations below 4 km. This issue will be further investigated in Part II using the LES simulations of the cirrus anvils.

Finally, in the past, attention has been primarily focused on CCN, and IFN to a lesser extent, when examining the impacts of aerosols on storm characteristics. The results shown here highlight the fact that the impacts of varying GCCN and IFN concentration are just as significant as those associated with CCN, and that they need to be considered when examining the impacts of nucleating aerosols, such as those found in Saharan dust, on convective storm characteristics. Also, all three nucleating aerosols affect the depth, microphysical characteristics, water mass, and organization of the anvil, which in turn will influence the radiative forcing by the anvil and the associated climatic effects. The microphysical and radiative variations that occur within the anvil as a result of changes in aerosol concentrations will be examined in Part II of this paper.

Acknowledgments. Susan van den Heever, Gustavo Carrió, and William Cotton were funded by NASA under Contracts NAG5-11507 and NNG04GG44G. Paul DeMott and Anthony Prenni were funded by NASA under Contract NAG5-11476. The following people are gratefully acknowledged: Darrel Baumgardner for providing the CAS data, James C. Wilson for the N-MASS data, Gregory Roberts and Timothy VanReken for supplying the CCN data, Johannes Verlinde and the NRL and NCAR flight crews for the P-3 radar data, Louis Nguyen for the visible satellite images, and Curtis Marshall for the use of his soil moisture code. The comments of the anonymous reviewers are also appreciated.

REFERENCES

Albrecht, B., 1989: Aerosols, cloud microphysics, and fractional cloudiness. *Science,* **245,** 1227–1230.

Andreae, M. O., D. Rosenfeld, P. Artaxo, A. A. Costa, G. P. Frank, K. M. Longo, and M. A. F. Silva-Dias, 2004: Smoking rain clouds over the Amazon. *Science,* **303,** 1337–1342.

Baumgardner, D., H. Jonsson, W. Dawson, D. O'Connor, and R. Newton, 2001: The cloud, aerosol and precipitation spectrometer (CAPS): A new instrument for cloud investigations. *Atmos. Res.,* **59-60,** 251–264.

Borys, R. D., D. H. Lowenthal, M. A. Wetzel, F. Herrera, A. Gonzalez, and J. Harris, 1998: Chemical and microphysical properties of marine stratiform cloud in the North Atlantic. *J. Geophys. Res.,* **103,** 22 073–22 085.

Braham, R. R., Jr., R. G. Semonin, A. H. Auer, S. A. Changnon Jr., and J. M. Hales, 1981: Summary of urban effects on clouds and rain. *METROMEX: A Review and Summary, Meteor. Monogr*., No. 40, Amer. Meteor. Soc., 141–152.

Carrió, G. G., S. C. van den Heever, and W. R. Cotton, 2006: Impacts of nucleating aerosol on anvil–cirrus clouds: A modeling study. *Atmos. Res.,* in press.

Cerveny, R. S., and R. C. Balling Jr., 1998: Weekly cycles of air pollutants, precipitation and tropical cyclones in the coastal NW Atlantic region. *Nature,* **394,** 561–563.

Chen, Y., S. M. Kreidenweis, L. M. McInnes, D. C. Rogers, and P. J. DeMott, 1998: Single particle analyses of ice nucleating particles in the upper troposphere and lower stratosphere. *Geophys. Res. Lett.,* **25,** 1391–1394.

Cotton, W. R., 1972: Numerical simulation of precipitation development in supercooled cumuli—Part I. *Mon. Wea. Rev.,* **100,** 757–763.

——, and Coauthors, 2003: RAMS 2001: Current status and future directions. *Meteor. Atmos. Phys.,* **82,** 5–29.

DeMott, P. J., K. Sassen, M. R. Poellet, D. Baumgardner, D. C. Rogers, S. D. Brooks, A. J. Prenni, and S. M. Kreidenweis, 2003: African dust aerosols as atmospheric ice nuclei. *Geophys. Res. Lett.,* **30,** 1732, doi:10.1029/2003GL017410.

Dessens, J., J. L. Sánchez, C. Berthet, and R. Fraile, 2004: Hailstone size distribution in atmospheric Saharan dust outbreaks. Preprints, *14th Int. Conf. on Clouds and Precipitation*, Bologna, Italy, ICCP, 63–65.

Dettwiller, J., and S. A. Changnon, 1976: Possible urban effects on maximum daily rainfall at Paris, St. Louis and Chicago. *J. Appl. Meteor.,* **15,** 517–519.

Dunion, J. P., and C. S. Velden, 2004: The impact of the Saharan Air Layer on Atlantic tropical cyclone activity. *Bull. Amer. Meteor. Soc.,* **85,** 353–365.

Eagan, R. C., P. V. Hobbs, and L. F. Radke, 1974: Particle emissions from a large Kraft paper mill and their effects on the microstructure of warm clouds. *J. Appl. Meteor.,* **13,** 535–552.

Feingold, G., W. R. Cotton, S. M. Kreidenweis, and J. T. Davis, 1999: The impact of giant cloud condensation nuclei on drizzle formation in stratocumulus: Implications for cloud radiative properties. *J. Atmos. Sci.,* **56,** 4100–4117.

Fridland, A. M., and Coauthors, 2004: Evidence for the predominance of mid-tropospheric aerosols as subtropical anvil cloud nuclei. *Science,* **304,** 718–722.

Gagin, A., 1965: Ice nuclei, their physical characteristics and possible effect on precipitation initiation. *Proc. Tokyo–Sapporo Int. Conf. on Cloud Physics,* Sapporo, Japan, Int. Association of Meterorology and Atmospheric Physics of the IUGG, 155–162.

Harrington, J. Y., 1997: The effects of radiative and microphysical processes on simulated warm and transition season Arctic stratus. Ph.D. dissertation, Colorado State University, 289 pp. [Available from Department of Atmospheric Science, Colorado State University, Fort Collins, CO 80523.]

Hill, G. E., 1974: Factors controlling the size and spacing of cumulus clouds as revealed by numerical experiments. *J. Atmos. Sci.,* **31,** 646–673.

Hindman, E. E., II, P. V. Hobbs, and L. F. Radke, 1977a: Cloud

condensation nuclei from a paper mill. Part I: Measured effects on clouds. *J. Appl. Meteor.,* **16,** 745–752.

——, P. M. Tag, B. A. Silverman, and P. V. Hobbs, 1977b: Cloud condensation nuclei from a paper mill. Part II: Calculated effects on rainfall. *J. Appl. Meteor.,* **16,** 753–755.

Hobbs, P. V., L. F. Radke, and S. E. Shumway, 1970: Cloud condensation nuclei from industrial sources and their apparent influence on precipitation in Washington State. *J. Atmos. Sci.,* **27,** 81–89.

Hung, H.-M., A. Malinowski, and S. Martin, 2003: Kinetics of heterogeneous ice nucleation on the surfaces of mineral dust cores inserted into aqueous sulfate particles. *J. Phys. Chem.,* **107A,** 1296–1306.

Isono, K., M. Komabayasi, and A. Ono, 1959: The nature and origin of ice nuclei in the atmosphere. *J. Meteor. Soc. Japan,* **37,** 211–233.

Jensen, E., D. Starr, and B. Toon, 2004: Mission investigates tropical cirrus clouds. *Eos, Trans. Amer. Geophys. Union,* **84,** 45–50.

Jiang, H., G. Feingold, and W. R. Cotton, 2002: Simulations of aerosol-cloud-dynamical feedbacks resulting from entrainment of aerosol into the marine boundary layer during the Atlantic Stratocumulus Transition Experiment. *J. Geophys. Res.,* **107,** 4813, doi:10.1029/2001JD001502.

Kaufman, Y. J., and T. Nakajima, 1993: Effect of Amazon smoke on cloud microphysics and albedo—Analysis from satellite imagery. *J. Appl. Meteor.,* **32,** 729–744.

Klemp, J. B., and R. B. Wilhelmson, 1978: The simulation of three-dimensional convective storm dynamics. *J. Atmos. Sci.,* **35,** 1070–1096.

Koenig, L. R., and F. W. Murray, 1976: Ice-bearing cumulus cloud evolution: Numerical simulations and general comparison against observations. *J. Appl. Meteor.,* **15,** 747–762.

Kuo, H. L., 1974: Further studies of the parameterization of the influence of cumulus convection on large-scale flow. *J. Atmos. Sci.,* **31,** 1232–1240.

Kushlan, J. A., 1990: Freshwater marshes. *The Ecosystems of Florida*, R. L. Meyers and J. J. Ewel, Eds., University of Central Florida Press, 324–363.

Laird, N. F., H. T. Ochs III, R. M. Rauber, and L. J. Miller, 2000: Initial precipitation formation in warm Florida cumulus. *J. Atmos. Sci.,* **57,** 3740–3751.

Lee, S.-H., and Coauthors, 2004: New particle formation observed in the tropical/subtropical cirrus clouds. *J. Geophys. Res.,* **109,** D20209, doi:10.1029/2004JD005033.

Levi, Y., and D. Rosenfeld, 1996: Ice nuclei, rainwater chemical composition, and static cloud seeding effects in Israel. *J. Appl. Meteor.,* **35,** 1494–1501.

Levin, Z., E. Ganor, and V. Gladstein, 1996: The effects of desert particles coated with sulfate on rain formation in the eastern Mediterranean. *J. Appl. Meteor.,* **35,** 1511–1523.

Lilly, D. K., 1962: On the numerical simulation of buoyant convection. *Tellus,* **14,** 148–172.

Mahowald, N. M., and L. M. Kiehl, 2003: Mineral aerosol and cloud interactions. *Geophys. Res. Lett.,* **30,** 1475, doi:10.1029/2002GL016762.

Marshall, C. H., R. A. Pielke Sr., L. T. Steyaert, and D. A. Willard, 2004: The impact of anthropogenic land-cover change on the Florida peninsula sea breezes and warm season sensible weather. *Mon. Wea. Rev.,* **132,** 28–52.

Mather, G. K., 1991: Coalescence enhancement in large multicell storms caused by the emissions from a Kraft paper mill. *J. Appl. Meteor.,* **30,** 1134–1146.

Mellor, G. L., and T. Yamada, 1974: A hierarchy of turbulence closure models for planetary boundary layers. *J. Atmos. Sci.,* **31,** 1791–1806.

Mesinger, F., and A. Arakawa, 1976: Numerical methods used in atmospheric models. GARP Publication Series 14, WMO/ICSU Joint Organizing Committee, 64 pp.

Meyers, M. P., P. J. DeMott, and W. R. Cotton, 1992: New primary ice nucleation parameterizations in an explicit cloud model. *J. Appl. Meteor.,* **31,** 708–721.

——, R. L. Walko, J. Y. Harrington, and W. R. Cotton, 1997: New RAMS cloud microphysics parameterization. Part II: The two-moment scheme. *Atmos. Res.,* **45,** 3–39.

Molinari, J., 1985: A general form of Kuo's cumulus parameterization. *Mon. Wea. Rev.,* **113,** 1411–1416.

Perry, K., T. Cahill, R. Eldred, D. D. Dutcher, and T. E. Gill, 1997: Long-range transport of North African dust to the eastern United States. *J. Geophys. Res.,* **102,** 11 225–11 238.

——, ——, R. Schnell, and J. Harris, 1999: Long-range transport of anthropogenic aerosols to the National Oceanic and Atmospheric Administration baseline station at Mauna Loa Observatory, Hawaii. *J. Geophys. Res.,* **104,** 18 521–18 533.

Pielke, R. A., and Coauthors, 1992: A comprehensive meteorological modeling system—RAMS. *Meteor. Atmos. Phys.,* **49,** 69–91.

Prospero, J. M., 1996: Saharan dust transport over the North Atlantic Ocean and Mediterranean: An overview. *The Impact of Desert Dust Across the Mediterranean*, S. Guerzoni and R. Chester, Eds., Kluwer Academic, 133–151.

——, 1999: Long-term measurements of the transport of African mineral dust to the southeastern United States: Implications for regional air quality. *J. Geophys. Res.,* **104,** 15 917–15 927.

——, and T. N. Carlson, 1972: Vertical and areal distributions of Saharan dust over the western equatorial North Atlantic Ocean. *J. Geophys. Res.,* **77,** 5255–5265.

Quijano, A. L., I. N. Sokolik, and O. B. Toon, 2000: Radiative heating rates and direct radiative forcing by mineral dust in cloudy atmospheric conditions. *J. Geophys. Res.,* **105,** 12 207–12 219.

Roberts, P., and J. Hallett, 1968: A laboratory study of the ice nucleating properties of some mineral particulates. *Quart. J. Roy. Meteor. Soc.,* **94,** 25–34.

Rogers, D. C., P. J. DeMott, S. M. Kreidenweis, and Y. Chen, 2001: A continuous flow diffusion chamber for airborne measurements of ice nuclei. *J. Atmos. Oceanic Technol.,* **18,** 725–741.

Rosenfeld, D., 1999: TRMM observed first direct evidence of smoke from forest fires inhibiting rainfall. *Geophys. Res. Lett.,* **26,** 3105–3108.

——, 2000: Suppression of rain and snow by urban and industrial air pollution. *Science,* **287,** 1793–1796.

——, and W. L. Woodley, 1989: Effects of cloud seeding in west Texas. *J. Appl. Meteor.,* **28,** 1050–1080.

——, and ——, 1993: Effects of cloud seeding in west Texas: Additional results and new insights. *J. Appl. Meteor.,* **32,** 1848–1866.

——, and R. Nirel, 1996: Seeding effectiveness—The interaction of desert dust and the southern margins of rain cloud systems in Israel. *J. Appl. Meteor.,* **35,** 1502–1510.

——, and I. M. Lensky, 1998: Satellite-based insights into precipitation formation processes in continental and maritime convective clouds. *Bull. Amer. Meteor. Soc.,* **79,** 2457–2476.

——, Y. Rudich, and R. Lahav, 2001: Desert dust suppressing

precipitation: A possible desertification feedback loop. *Proc. Natl. Acad. Sci. USA,* **98,** 5975–5980.

——, R. Lahav, A. Khain, and M. Pinsky, 2002: The role of sea spray in cleansing air pollution over ocean via cloud processes. *Science,* **297,** 1667–1670.

Saleeby, S. M., and W. R. Cotton, 2004: A large-droplet mode and prognostic number concentration of cloud droplets in the Colorado State University Regional Atmospheric Modeling System (RAMS). Part I: Module descriptions and supercell test simulations. *J. Appl. Meteor.,* **43,** 182–195.

Sassen, K., 2002: Indirect climate forcing over the western US from Asian dust storms. *Geophys. Res. Lett.,* **29,** 1465, doi:10.1029/2001GL014051.

——, P. J. DeMott, J. M. Prospero, and M. R. Poellet, 2003: Saharan dust storms and indirect aerosol effects on clouds: CRYSTAL-FACE results. *Geophys. Res. Lett.,* **30,** 1633, doi:10.1029/2003GL017371.

Schaefer, V. J., 1949: The formation of ice crystals in the laboratory and the atmosphere. *Chem. Rev.,* **44,** 291–320.

——, 1954: The concentrations of ice nuclei in air passing the summit of Mt. Washington. *Bull. Amer. Meteor. Soc.,* **35,** 310–314.

Scott, B. C., and P. V. Hobbs, 1977: A theoretical study of the evolution of mixed-phase cumulus clouds. *J. Atmos. Sci.,* **34,** 812–826.

Simpson, J., G. W. Brier, and R. H. Simpson, 1967: STORMFURY cumulus seeding experiment 1965: Statistical analysis and main results. *J. Atmos. Sci.,* **24,** 508–521.

Smagorinsky, J., 1963: General circulation experiments with the primitive equations. I. The basic experiment. *Mon. Wea. Rev.,* **91,** 99–164.

Squires, P., 1956: The microstructure of cumuli in maritime and continental air. *Tellus,* **8,** 443–444.

——, 1958: The microstructure and colloidal stability of warm clouds. Part I: The relation between structure and stability. *Tellus,* **10,** 256–261.

Stein, U., and P. Alpert, 1993: Factor separation in numerical simulations. *J. Atmos. Sci.,* **50,** 2107–2115.

Straka, W. C., 2004: Calculations of precipitation and anvil efficiencies during CRYSTAL-FACE using the ELDORA dual-Doppler radar. M.S. thesis, Dept. of Atmospheric Science, Colorado State University, 91 pp. [Available from Department of Atmospheric Science, Colorado State University, Fort Collins, CO 80523.]

Twomey, S., 1977: The influence of pollution on the shortwave albedo of clouds. *J. Atmos. Sci.,* **34,** 1149–1152.

——, M. Piepgrass, and T. L. Wolfe, 1984: An assessment of the impact of pollution on global cloud albedo. *Tellus,* **36B,** 356–366.

VanReken, T. M., T. A. Rissman, G. C. Roberts, V. Varutbangkul, H. H. Jonsson, R. C. Flagan, and J. H. Seinfeld, 2003: Toward aerosol/cloud condensation nuclei (CCN) closure during CRYSTAL-FACE. *J. Geophys. Res.,* **108,** 4633, doi:10.1029/2003JD003582.

Walko, R. L., and Coauthors, 2000: Coupled atmosphere–biophysics–hydrology models for environmental modeling. *J. Appl. Meteor.,* **39,** 931–944.

Warner, J., and S. Twomey, 1967: Comparison of measurements of cloud droplets and cloud nuclei. *J. Atmos. Sci.,* **24,** 702–703.

Zuberi, B., A. Bertram, C. Cassa, L. Molina, and M. Molina, 2002: Heterogeneous nucleation of ice in $(NH_4)_2SO_4$-H_2O particles with mineral dust immersions. *Geophys. Res. Lett.,* **29,** 1504, doi:10.1029/2001GL014289.